Innovative Laser-based Methods for Monitoring Fuel Retention in ITER

A. Huber[1], Ph. Andrew[2], G. Sergienko[1], J. Assmann[1], D. Castano[1], A. De Schepper[1], S. Friese[1], R. Greven[3], I. Ivashov[1], D. Kampf[4], Y. Krasikov[1], C. C. Klepper[5], H. T. Lambertz[1], Ph. Mertens[6], K. Mlynczak[1], G. Offermanns[3], B. Quinlan[5], K. Rasinska[1], M. Schrader[1], D. Van Staden[4], A. Terra[1], Xi Jiang[2], M. Zlobinski[1], V. Huber[7], A. Reutlinger[4], S. Brezinsek[1], Ch. Linsmeier[1]

[1]*Institute of Fusion Energy and Nuclear Waste Management–Plasma Physics, Forschungszentrum Jülich GmbH, Germany*

[2]*ITER Organization, Route de Vinon, CS 90 046, 13067 Saint-Paul-lez-Durance, France*

[3]*Forschungszentrum Jülich GmbH, Institute of Technology and Engineering, 52425 Jülich, Germany*

[4]*KTO Kampf Telescope Optics GmbH, 81379 Munich, Germany*

[5]*Oak Ridge National Laboratory, Oak Ridge, TN 37831-6169, USA*

[6]*FUSE-L Fusion Specific Expertise-Liege, 4031 Liège, – Belgium*

[7]*Forschungszentrum Jülich GmbH, Supercomputing Centre, 52425 Jülich, Germany*

E-mail: A.Huber@fz-juelich.de

Keywords: Tritium retention, Laser diagnostic, Hydrogen isotopes, In situ monitoring, Plasma-material interactions

Abstract:

This paper addresses the challenge of tritium inventory management in ITER and future fusion reactors, highlighting the importance of accurate tritium measurement and its spatial distribution within the vacuum vessel. Given ITER's operational constraints, especially the limit on tritium retention, precise measurement is essential for both safety and regulatory compliance. To tackle these questions, the paper presents the T-monitor diagnostic system developed by Forschungszentrum Jülich, which uses Laser-Induced Desorption (LID) in combination with Diagnostic Residual Gas Analysis (DRGA) to measure hydrogen isotope concentrations on the surface of divertor tiles. The system integrates a high-power laser, advanced optical components, and a Fast Scanning Mirror Unit (FSMU) for accurate laser spot positioning with rapid response.

Designed to measure *in situ* tritium retention, the diagnostic provides high-resolution spatial mapping, vital for evaluating detritiation strategies. The laser heating process increases the divertor surface temperature to 1600 K within the laser spot, promoting hydrogen isotope desorption. Accurate measurements require the precise control of laser parameters, including pulse duration and spot size, with a target relative accuracy of 20%. The optical design includes both in-vessel and ex-vessel components, such as durable high-reflectivity mirrors made of gold and copper, selected not only for their infrared performance but also for their transmission of visible wavelengths for observation purposes. To protect optical components from contamination, a pneumatic shutter is used.

1. Introduction

One of the most serious challenges for the operation of ITER and future fusion devices is the control of the inventory of tritium (T) stored inside the vacuum vessel. Maintaining a safe and manageable level of tritium is essential, as its accumulation poses significant safety and regulatory risks. As a licensed nuclear facility, ITER is required to limit tritium retention to minimize the potential for accidental releases. This constraint is defined by a maximum allowable tritium inventory of 1 kg, which includes 120 g of tritium trapped in the divertor cryopumps and 180 g of measurement uncertainty, leaving a strict retention limit of 700 g within the vessel components [1]. Ensuring compliance with these limits necessitates robust, precise, and non-invasive diagnostic systems capable of real-time monitoring of the tritium distribution and accumulation.

A key challenge lies in monitoring tritium retention without removing wall components, a so-called *in-situ* approach. To address this, Forschungszentrum Jülich has proposed a laser-based T-monitor diagnostic system for ITER, capable of remotely determining the tritium content in the deposited layers on the inner divertor tiles. Tritium accumulation in these layers arises from complex plasma-material interactions, including the erosion of wall materials and co-deposition of hydrogen isotopes alongside redeposited material.

In early 2023, ITER Organization (IO) initiated a re-baselining exercise, with one of the key components being the transition of the first wall material from beryllium to tungsten (W) [2]. The advantages of using tungsten include a lower sputtering yield, higher energy threshold, improved erosion lifetime, a higher melting point, and greater resilience during disruptions. However, this transition increases the tungsten plasma-facing surface area, raising the risk of a higher tungsten content in the core plasma which could result in radiative losses and poses challenges in maintaining the H-mode. Additionally, replacement of beryllium reduces impurity gettering, particularly for oxygen, which could complicate the plasma start-up. To address these issues, a boronization process will be applied to the first wall, although this may lead to increased tritium fuel retention due to co-deposition with boron.

In full-tungsten devices, a thin boron (B) coating is typically applied to plasma-facing components (PFCs) through glow discharge plasma-assisted chemical vapor deposition (boronization), which helps with plasma initiation and start-up. However, in ITER, this method carries the risk of increased tritium fuel retention, as eroded boron may co-deposit with the fuel.

In devices with low-Z materials in the main chamber, the hydrogen isotope content primarily builds up through the erosion of these low-Z materials and the co-deposition of hydrogen isotopes, particularly in magnetically shadowed regions [3] and on the inner tungsten divertor [4]. However, in a "full tungsten" ITER, the main sources of tritium retention will shift to the co-deposition of hydrogen isotopes with eroded and re-deposited boron (B) and tungsten (W), as well as implantation into the tungsten material [2]. As boron is eroded, it is expected to migrate and deposit at the divertor [5]. It should be noted that the boron source can be more accurately quantified, particularly the boron introduced by boronization [6]. As previously noted, in a full tungsten machine, the B coating replaces the oxygen-gettering role of Be through boronization, although the coating is relatively short-lived.

The measurement concept relies on laser-induced desorption (LID) to release tritium-containing gases from surfaces, followed by detection using Residual Gas Analysis (RGA). The LID-QMS (Laser-Induced Desorption combined with Quadrupole Mass Spectrometry) diagnostic method has been validated both *ex situ* in laboratory experiments [7] and *in situ* in operational fusion devices such as TEXTOR [8,9] and JET [10]. This approach enables the acquisition of precise, spatially resolved retention maps and facilitates the assessment of detritiation methods with localized precision. In contrast to campaign-integrated measurements, LID-QMS provides close to real-time insights into fuel retention dynamics, enhancing operational flexibility.

Beyond diagnostics, this system advances the understanding of tritium retention physics, offering insights into processes such as surface erosion, material redeposition, and hydrogen isotope interactions. It also supports optimization of wall materials and operational protocols, addressing the long-term requirements for safe and efficient fusion reactor operation. By combining diagnostic precision with a comprehensive understanding of retention mechanisms, the proposed system aligns with ITER's safety goals and lays the groundwork for scalable solutions in future fusion devices.

This article presents an optical design that employs a high-power laser and metallic mirrors for efficient NIR beam transport and coaxial observation in the VIS/NIR (visible/near-infrared) spectral ranges. The mirrors use Zerodur or CuCrZr substrates with gold (Au) coatings, chosen to withstand ITER's harsh nuclear environment. Unlike conventional dielectric coatings, gold provides a broad spectral reflectivity across the VIS and NIR ranges. It is highly resistant to radiation-induced degradation and thermal stresses. The design addresses both the detection limits and the functional requirements of the T-Monitor diagnostic system. In this overview paper, we provide a technical and scientific description of the T-Monitor diagnostic.

The structure of this article is organized as follows: Section 1 begins by addressing the challenges related to managing tritium inventory in ITER and future fusion reactors, focusing on the need for accurate tritium measurement and spatial distribution within the vacuum vessel. Section 2 discusses the approach and measurement requirements for the T-monitor diagnostic on ITER, including the analysis of laser spot sizes and their impact on measurement accuracy, as well as the field of view of the scanning area. Section 3 introduces the ITER Residual Gas Analyzer System. Section 4 presents the optical design of the T-monitor, detailing components inside the port plug, Interspace Support Structure (ISS) area, port cell, and the T-building, along with a discussion of the mechanical components. Section 5 highlights the laser power, mirror materials, and other requirements necessary for precise measurements. Section 6 focuses on the thermal stresses induced by laser heating on the mirrors and the selection of appropriate materials for the optical system. In Section 8, the importance of monitoring the transmittance of the optical system is addressed through the use of black body calibration and calorimeter systems to ensure optimal performance. Additionally, surface temperature measurements under harsh conditions, including the presence of dust and deposited layers, are discussed. Finally, Section 9 provides a summary and conclusion, emphasizing the critical role of accurate tritium measurements for the success of ITER and future fusion reactors.

2. The approach and measurement criteria

2.1 Principle of operation of the laser-induced desorption tool

The fundamental concept behind laser-based LID-QMS diagnostics is to heat specific regions of the first wall surface using intense laser radiation between plasma discharges, under vacuum conditions (see Fig. 1). The laser pulse must generate peak temperatures high enough to desorb all hydrogen isotopes and their compounds from the surface layer in a single laser pulse. This desorption releases wall particles, including atoms and molecules, which are then detected by Diagnostic Residual Gas Analysis (DRGA). A Quadrupole Mass Spectrometer (QMS) is primarily used to quantify the rapid partial pressure changes in specific mass-to-charge ratios (m/q = 3, 4, 5, and 6). This diagnostic technique is referred to as LID-QMS. A detailed description of the RGA system intended for use on ITER is provided in Section 3.0 and further elaborated in [11].

When applied as an *in-situ* diagnostic tool, LID-QMS offers several advantages:

Real-time Retention Analysis: Provides direct insights into retention physics over short timescales, as opposed to relying on campaign-integrated measurements.

Spatially Resolved Mapping: Enables the creation of detailed fuel retention maps of the wall.

Effectiveness of detritiation methods: Assesses the spatially resolved efficiency of detritiation methods, facilitating targeted improvements in fuel management and wall conditioning techniques.

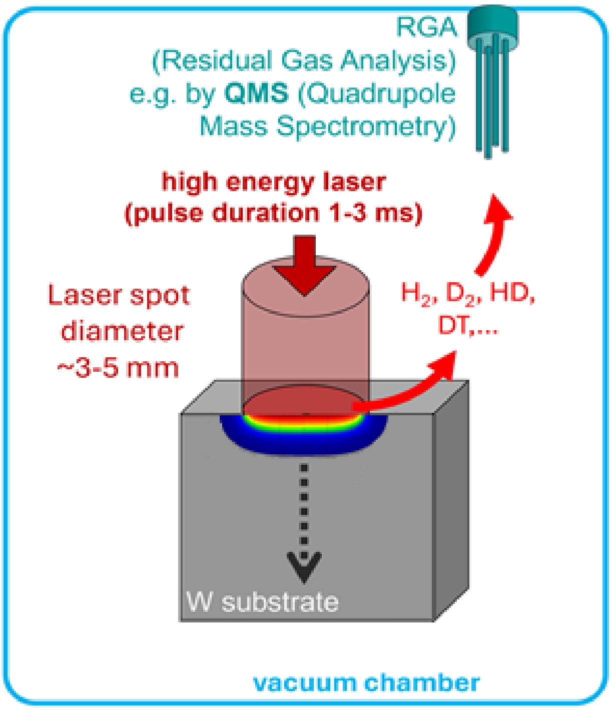

Fig.1: Operating principle of the laser-induced desorption tool.

On the other hand, achieving precision in controlling laser parameters —such as wavelength, intensity, and pulse duration— poses a significant challenge in laser-based diagnostics and material processing. These parameters must be meticulously adjusted to fulfil the following critical requirements:

Target Specific Layers or Depths: Achieving the desired depth of material interaction (e.g., surface desorption or penetration into a deposited layer) requires fine-tuning the laser's energy delivery. For instance, the pulse duration must allow sufficient heat penetration for desorption without overheating surrounding material layers, such as tungsten in ITER applications.

Avoiding Damage to Substrates: Excessive energy can cause unintended effects, including surface melting, ablation, or bulk material damage. Controlling the spatial energy distribution ensures precision and minimizes collateral damage to the underlying or adjacent materials.

Maintaining Uniformity: Achieving a uniform laser energy distribution over the spot size is essential for ensuring consistent desorption and accurate measurement results. To meet the required accuracy, the spatial power inhomogeneity must not exceed 20% of the average power.

Fig. 2 shows the spatial distribution of the laser intensity measured during the LID-QMS experiment in the laboratory [12] using a video camera. The fiber output (diameter 400 µm, NA=0.2) is imaged onto the sample surface using a lens of 6 cm focal length and 30 mm diameter. The fiber-to-lens distance is ≈7.6 cm, and the lens-to-sample distance is 56.8 cm, yielding a 3 mm spot diameter with an approximately top-hat power-density profile and a peak intensity of ≈500 MW/m². Beam alignment, stability, and quality are carefully controlled to maintain the uniform irradiation.

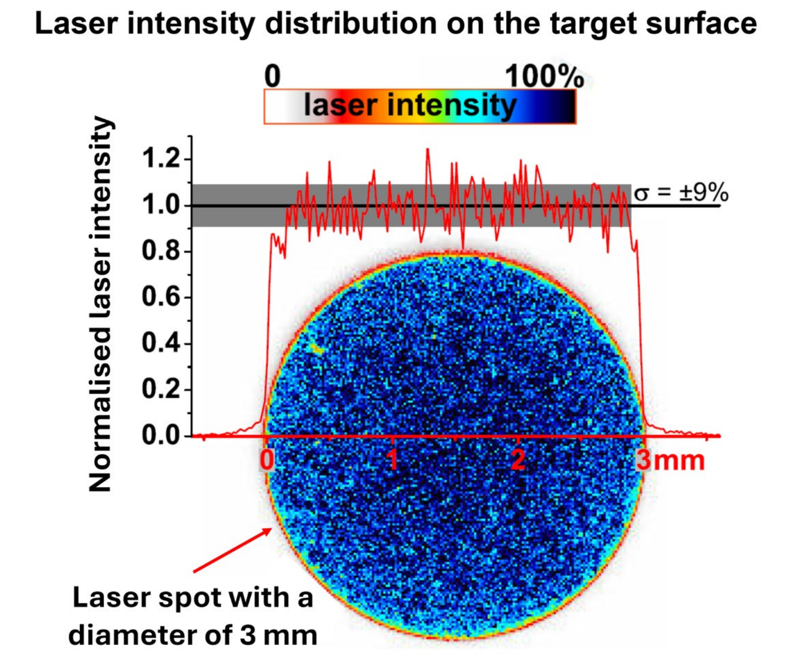

Fig.2 Spatial distribution of laser intensity measured during the LID-QMS experiment in the laboratory. This figure is reproduced from [12].

2.2 The Laser Heating Process

If the laser heat flux, q, is applied at a constant rate to the divertor tile for a laser pulse duration of τ, the temperature at depth δ and time t is given by the following equation [13]:

$$T(\delta,t) = \frac{4q\sqrt{\kappa t}}{K\sqrt{\pi}} \int_{\frac{z}{2\sqrt{\kappa t}}}^{\infty} \int_{u}^{\infty} \exp\left(-\xi^2\right) d\xi du \quad (1)$$

where K is the thermal conductivity, and κ is the thermal diffusivity. The thermal diffusivity κ is related to the other thermal parameters by $\kappa = {K}/{C_p\rho}$, where C_p is the heat capacity of the divertor tile, and ρ is the material density.

Therefore, the analytical formula for the semi-infinite medium describes the temperature profile as a one-dimensional spatial function dependent on the depth δ:

$$T(\delta,t) = \frac{2q}{K}\sqrt{\frac{\kappa t}{\pi}}\left(e^{-\frac{z^2}{4\kappa t}} - \sqrt{\pi}\frac{z}{2\sqrt{\kappa t}}erfc(\frac{z}{2\sqrt{\kappa t}})\right) = T(0,t)\left(e^{-\frac{z^2}{4\kappa t}} - \sqrt{\pi}\frac{z}{2\sqrt{\kappa t}}erfc(\frac{z}{2\sqrt{\kappa t}})\right) \quad (2)$$

Fig. 3 shows (a) a schematic representation of laser illumination on the divertor target, indicating lateral heat propagation within the target, and (b) the temperature distribution in the divertor target at the end of the laser pulse duration. The heat penetration depth in the tungsten divertor target can be estimated to 0.26 mm for a 1 ms pulse duration and 0.45 mm for a 3 ms pulse duration.

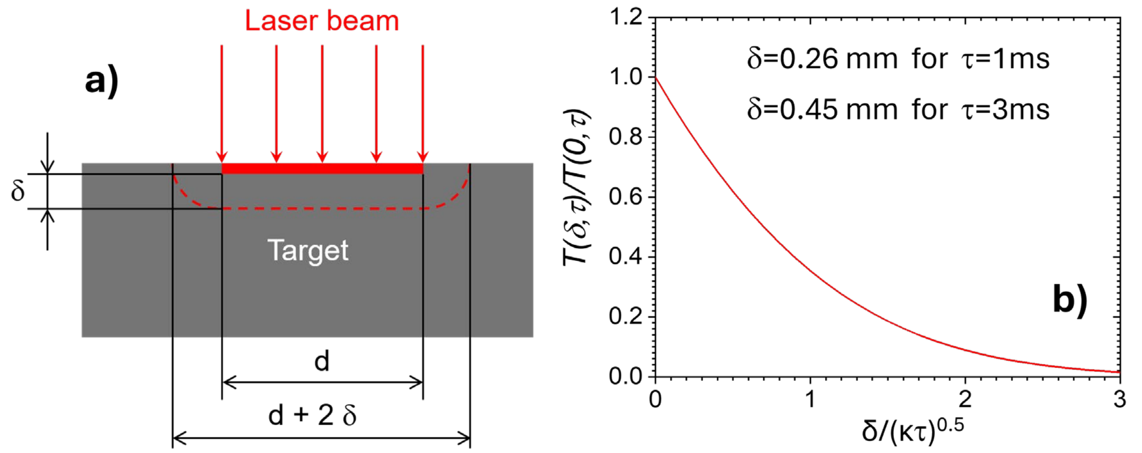

Fig. 3: a) Schematic of the laser illumination of the divertor target. b) Temperature distribution in the divertor target at the end of the laser pulse duration, showing the characteristic thermal penetration depth δ, which indicates how far heat has diffused into the material during the pulse.

To ensure the surface reaches 1600 K, the power density and pulse duration must be sufficiently high. At this temperature, all hydrogen isotopes are fully desorbed from the expected deposited layer, based on prior experience. For the deposited layers in TEXTOR and JET, hydrogen isotopes are typically implanted to depths of 10–50 µm, with desorption times limited by the ms-scale laser pulse duration. For ITER-relevant tungsten surfaces, implantation depths (i.e., the deposition layer thickness) are expected to be ≈100 µm. Calculations of the heat diffusion length in tungsten for pulse durations of 1 ms and 3 ms indicate that the heat penetrates well beyond the ~100 µm layer, meaning the entire layer is heated rapidly. Therefore, the applied laser pulses (1–3 ms) are sufficient to heat the entire implanted layer, ensuring fast desorption.

Additionally, the diffusion coefficient of hydrogen isotopes increases exponentially with temperature, so desorption begins during the laser pulse and continues shortly after the pulse ends. The dynamics of absorption and desorption are expected to be similar under ITER conditions, although neutron-induced displacement damage may locally increase hydrogen retention [14–16]. A temperature of 1600 K is adequate for desorbing the entire hydrogen isotope content from both Be:D and B:D deposition layers [7,8.9,10]. Notably, the first laser desorption experiments were conducted on B:D deposited layers in TEXTOR [8]. In these experiments, a laser pulse with a duration of 0.3 ms and energy of 5 J completely released the D content from a B:D layer, covering a spot area of about 0.4 cm^2. This corresponds to a maximum absorbed power density of approximately 415 MW/m^2. On the other hand, thermal heating must not exceed the melting point of bulk tungsten (3695 K) to prevent significant sublimation of the tungsten material. To achieve a surface temperature of 1600 K on a 5 mm spot, the required absorbed power density is roughly 665 MW/m^2 for a 1 ms pulse and around 380 MW/m^2 for a 3 ms pulse.

The calculations were conducted for tungsten, assuming a laser absorption power fraction of 0.5. This value is based on laboratory measurements with tungsten samples at a near-infrared (NIR) laser wavelength of λ = 1.07 μm. For polished tungsten, the emissivity, and hence the fraction of absorbed laser power, is about 0.43 at a surface temperature of 1000 °C and λ = 1.07 μm [18]. The emissivity depends strongly on surface temperature and roughness. On ITER, the tungsten surfaces in the divertor will have significant roughness due to plasma exposure, and the surface roughness is known to increase the effective emissivity [19]. Taking this into account, a value of 0.5 is a reasonable estimate for the laser absorption fraction under ITER-relevant conditions. It should be emphasized that this is only an approximate value; the precise absorption fraction is not critical for the current analysis because if the laser power at the target were insufficient to reach the desired surface temperature, the laser power could be adjusted accordingly.

According to TMAP-7 modeling [17], when using a heating duration of 1 ms, the simulation predicts approximately 90% of the D will be released at a surface temperature of 1450 K. The amount of released D is expected to depend on the steady-state exposure temperature of W during D implantation, which will be addressed in future studies. It should be noted that if a single pulse is insufficient to desorb all the fuel, multiple pulses might be applied. Retention in the erosion zone of pure tungsten could be influenced by neutron irradiation, with the effect varying significantly depending on the level of irradiation damage, which is quantified in displacements per atom (dpa). At ITER's end-of-life, the estimated maximum damage values for tungsten at the inner divertor target are about 0.54 dpa [14]. According to [16], retention tends to increase with the presence of displacement damage. It was found [15,16] that at a damage dose of 0.23 dpa, the maximum deuterium concentration reaches approximately 1.4 at%, which is much lower than the fuel concentration anticipated in the boron layer. Nonetheless, measurements with the T-monitor diagnostic in the erosion zone of pure tungsten are expected.

2.3 The measurement requirements

The T-monitor diagnostic must be capable of measuring the surface tritium concentration at $n_{surf} = 2.1 \times 10^{21}$ T atoms/m², with an accuracy of 20% relative to the value [20]. These measurements will be performed on the inner divertor baffle, and these requirements are independent of the first wall material selection. The overall tritium content within the vacuum vessel can be determined by combining the tritium inventory measurements with codes such as the Monte Carlo-based ERO2.0 [21] or WallDYN [5].

For a full tungsten device, the primary contributors to tritium retention will be co-deposition with eroded and re-deposited boron and tungsten, as well as tritium implantation into tungsten. Simulations related to boron co-deposits and migration are detailed in paper [2]. To ensure conservative estimates for tritium retention in ITER, the ratio of {H/D/T}/B = 0.5 is assumed. Boron co-deposits can retain up to 4, 8, and 12 grams of H, D, and T, respectively, per 50 nm of boronization, corresponding to a deposition of 86 grams of boron (refer to Section 4.2 in [2]). Based on these values, the projected tritium retention in boron co-deposits is estimated to fall between 320 and 380 grams by the end of the DT-1 phase. This range reflects potential variations due to decisions made during the FPO-4 and 5 campaigns [2].

To determine the T content, partial pressures of all T containing gases must be measured: H_2, D_2, T_2, DT, HT, He (^{3}He and ^{4}He) , NH_3, ND_3, NT_3, NHD_2, NH_2D, NHT_2, NH_2T, NDT_2, ND_2T, H_2O, HDO, D_2O, HTO, DTO, and T_2O. As a compromise, a minimum of six required RGA mass channels should be selected: m/e = 1, 2, 3, 4, 5, and 6.
RGA requirements are as follows:

Time Response: The RGA should have a time response that is at least 1/10 of the vacuum vessel pumping time, which is approximately 20 seconds for ITER. This ensures rapid detection of gases during the operational cycle.
Resolution: The RGA must have sufficient resolution to effectively discriminate between the various gases listed above. This is crucial for distinguishing isotopes and compounds with closely related masses and for ensuring accurate measurements of tritium and other species.
These requirements ensure that the RGA system can provide precise and timely measurements of the gas species relevant to ITER's operational safety and diagnostics.

2.4 Selection of the optimal laser pulse duration

The selection of the laser pulse duration is crucial in achieving the required accuracy in tritium inventory measurements. Generally, the pulse duration should be kept as short as possible to minimize the effect of lateral heat propagation on the desorption area.

On the other hand, the heat penetration depth needs to be adequate to desorb fuel from the deposited layer, which is anticipated to be around 100 µm for a beryllium material configuration in ITER [1]. In contrast, for a full-W configuration, the expected depth of the deposited layer is smaller [2]. In this project, the laser parameters, based on a maximum coating layer thickness of 100 µm, are applicable to both material configurations, ensuring the diagnostic method is universally suitable.

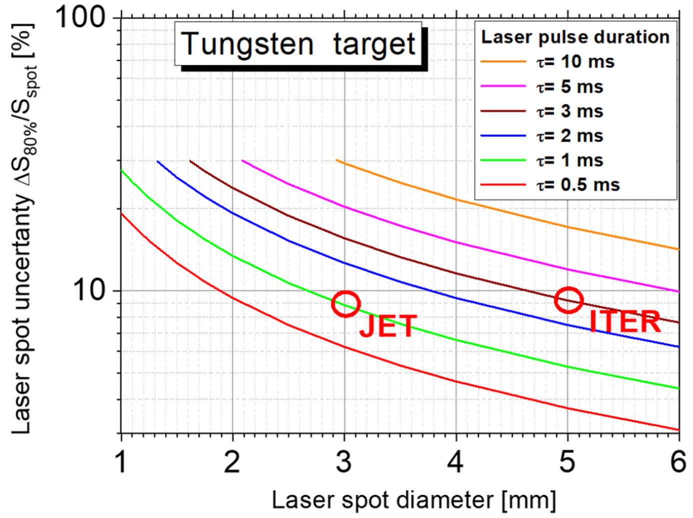

Fig. 4: Dependence of the uncertainty of the spot area on the laser spot size for different laser pulse durations.

Fig. 4 illustrates the operational parameter space for the laser, expressed in terms of spot diameter and uncertainty for different pulse durations. The uncertainty is defined as $\Delta S/S_{las} = (S_{heat}-S_{las})/S_{las}$, where S_{las} represents the laser spot area and S_{heat} is the heated area, which includes the region affected by lateral heat propagation, where the temperature T exceeds 80% of the maximum temperature in the illuminated spot.

From this operational space, it can be observed that a 5 mm laser spot and pulse durations between 1 ms and 3 ms are necessary to achieve a measurement uncertainty of less than 10%, with a spatial resolution of approximately 5 mm required for single-point measurements.

2.5 Scanning area for the LID-QMS Application

This system enables the measurement of thermally released gases from various locations within the vacuum vessel, offering spatially resolved data critical for understanding fuel retention and wall interactions. To achieve the required spatial resolution for tritium content measurements on ITER, two measurement points are needed in the poloidal direction on the same monoblock, and at least six points in the toroidal direction on the same toroidal monoblock. Given that the divertor monoblock measures about 12 mm by 31 mm (in the poloidal and toroidal directions) [22], the laser spot size must be 5 mm in diameter or smaller.

The measurement requirements for the T-monitor diagnostic are as follows: the diagnostic must measure the concentrations of protium (H), deuterium and tritium at the inner baffle, where co-deposits are primarily anticipated. The scanning area spans approximately 0.54 m in the poloidal direction and 0.11 m in the toroidal direction, as depicted in Fig. 5. It is important to

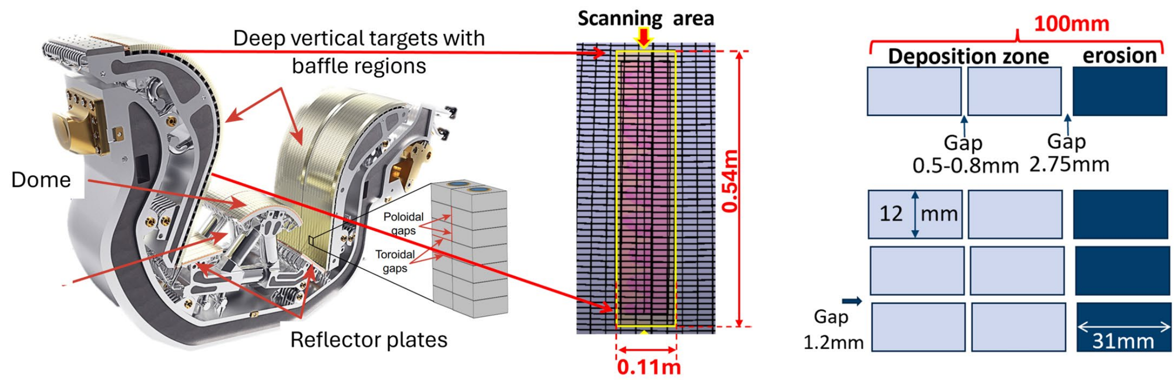

Fig. 5: A single ITER tungsten (W) divertor cassette, highlighting the scanning area on the inner divertor baffle. On the right-hand side is the schematic representation of the field of view (FoV), including the sizes of the gaps between the individual monoblocks

note that the toroidal extension should cover three monoblocks: two located in the deposition zone and one in the erosion zone. Measurements should be conducted outside of plasma pulses, under optimal vacuum conditions. The expected tritium concentration ranges from 10^{21} to 2×10^{24} m^{-2}.

3.0 ITER Residual Gas Analyzer System

The Diagnostic Residual Gas Analyzer (DRGA) system on ITER is designed to play a critical role in monitoring the composition of gases within the vacuum vessel, including isotopes of hydrogen (H, D, T), ^{3}He and ^{4}He (fusion ash), and impurities. It supports ITER's operational needs for machine protection, plasma control, and fusion research. The key features and requirements of the ITER DRGA system include:

Measurement Capability: The RGA will monitor fuel ratios (deuterium, tritium), helium isotopes, and other impurities. It integrates quadrupole mass spectrometry, ion trap mass spectrometry, and optical Penning discharge gauges to provide comprehensive diagnostic data.

Time Resolution: The DRGA system located in the lower diagnostic port (close to the divertor area) is optimized for a response time of approximately 1 second, even with an 8-meter separation between the diagnostic station and the sampled location in the vacuum vessel. This ensures real-time monitoring of gas dynamics and supports the time-sensitive demands of fusion plasma experiments.

Isotopic Resolution: The RGA can resolve isotopic differences to track tritium concentrations effectively, crucial for safe operations and regulatory compliance. Enhanced resolution also supports studies of plasma-wall interactions and isotope exchange phenomena.

Integration with ITER: The system includes advanced pumping and analysis methods to handle gas sampling under ITER's challenging operational conditions. Testing of prototypical components was performed on other fusion devices, such as JET and Wendelstein 7-X, providing valuable insights for ITER-specific challenges.
This RGA system represents a sophisticated blend of mass spectrometric and optical techniques, tailored for ITER's demanding environment, ensuring accurate and reliable diagnostics throughout its operational phases. For more technical details, the reader can explore the references from the Oak Ridge National Laboratory and related sources [e.g. ref. 11].

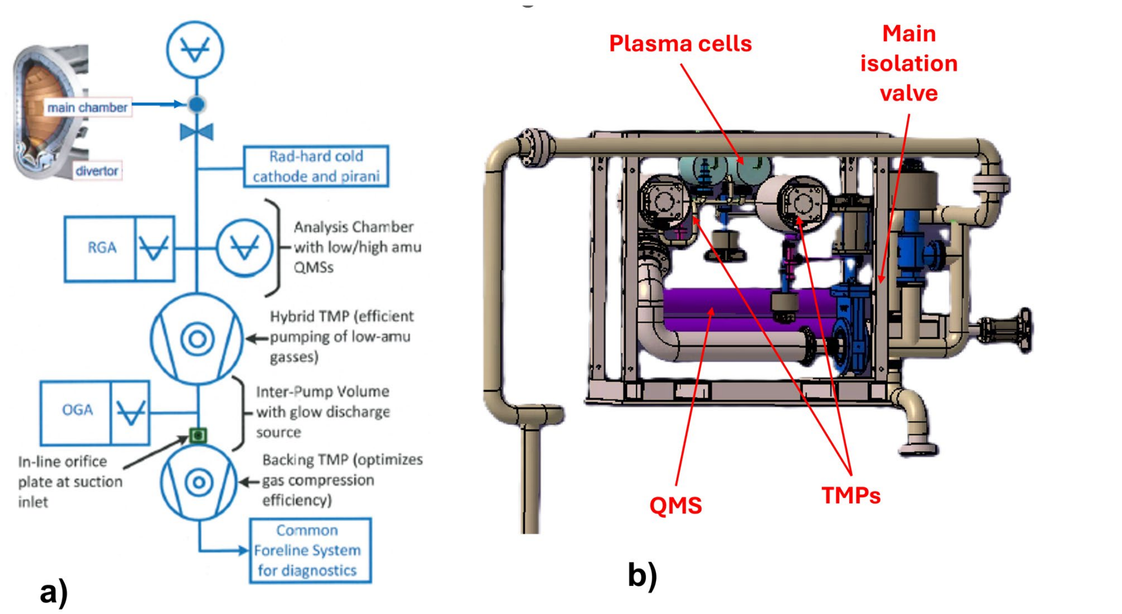

Fig. 6. RGA-OGA arrangement of the ITER DRGA system: a) schematic view and b) mechanical layout.

Fig. 6 illustrates the schematic of the Diagnostic Residual Gas Analyzer (DRGA) concept for ITER, which is to be installed in the equatorial plane [23]. The system incorporates several sensors, including a quadrupole mass spectrometer (QMS), ion-trap mass spectrometer (ITMS), optical gas analyzer (OGA), and total pressure measurement (TPM) sensors. The OGA is connected to an inter-stage port of the turbomolecular pump to accommodate higher working pressures.

Fig. 7 illustrates an example of the RGA signal, specifically the partial pressure of mass 3, which corresponds to HD molecules, during laser illumination of the samples in the lab. The laser illumination causes a sharp increase (Δp) in the pressure signal, followed by an exponential decay. The time constant of this decay is dependent on the pumping speed. To calculate the total number of released particles in a volume V during an injection process, where the partial pressure increases due to laser-induced desorption and decreases exponentially during pumping, we need to relate these changes in pressure to the number of particles released. The relationship between the pressure and the number of particles in a volume V is given by the ideal gas law:

$$N(t) = \frac{P(t)\,V}{k_B T_{FW}}$$

Where $P(t)$ is the pressure at time t, $N(t)$ is the number of particles at time t, k_B is the Boltzmann constant, T_{FW} is the temperature of the first wall.

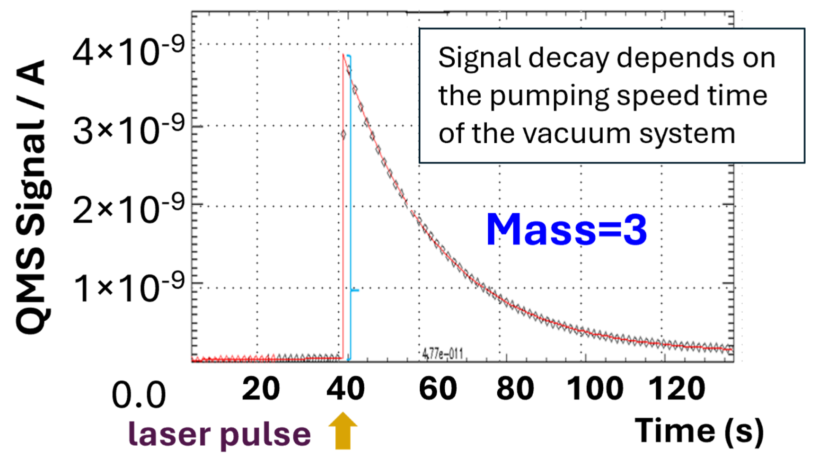

Fig 7 RGA signal during laser illumination.

The rate of change of pressure due to pumping is related to the pumping speed *S*. The pumping speed is the volume flow rate at which particles are removed from the vacuum vessel. The pumping speed at ITER is about 20 s. Therefore, the rate of change of the number of particles is:

$$\frac{dN(t)}{dt} = -\frac{S}{V}N(t)$$

This equation describes the exponential decrease in the number of particles due to pumping. Solving the differential equation, we obtain:

$$N(t) = N_0 e^{-\frac{S}{V}t}$$

where N_0 is the initial number of particles at time $t=0$.

The number of released molecules is thus determined by:

$$N_i = \frac{S_i}{k_B T_{FW}} \int P_i(t)dt$$

Where N_i is the number of molecules of species i, S_i the pumping speed of this molecular species, T_{FW} is the temperature of the first wall and P_i is the partial pressure of species i.

The rise time shown in Fig. 7 is determined primarily by the time response of the RGA system. As specified earlier, the RGA is required to have a time response at least one order of magnitude shorter than the vessel pumping time (≈20 s) to ensure a measurement accuracy better than 10%. Consequently, the rise time of the RGA signal expected on ITER is on the order of a fraction of a second to a few tenths of a second, and therefore much shorter than the characteristic pumping time.

The sensitivity of the QMS in the LID-QMS configuration is determined primarily by the effective conductance of the vacuum path connecting the interrogation point to the DRGA. In ITER, the QMS is connected to the main vacuum vessel through a dedicated diagnostic line, and the measured ion signal depends on (i) the total volume of the vessel, (ii) the conductance of the diagnostic path, and (iii) the pumping conditions during the laser pulse.

To determine the quantitative sensitivity and establish the limit of detection (LOD), the DRGA system will be calibrated in situ. Calibration is performed by injecting short, well-defined gas pulses with a known number of molecules into the vessel and recording the resulting partial-pressure transients at the QMS. The injected amounts are chosen to be comparable to the expected releases from a single LID pulse, ensuring that the system response is representative of the actual measurement regime.

This calibration procedure allows for the direct determination of:

- the transfer function of the vacuum line (i.e., how much of the released gas reaches the QMS as a function of conductance and chamber volume),
- the absolute sensitivity for the relevant mass-to-charge ratios (m/q = 3–6), and
- the effective LOD under ITER operating conditions.

In addition to these vacuum-system parameters, the effective LOD also depends on the desorption area, and thus on the selected LID operation mode (the modes are presented and discussed in Section 8), since different pulse numbers and fluences release different total amounts of gas. This operational dependence, and its implications for meeting the required surface-tritium sensitivity of $n_{surf} = 2.1 \times 10^{21}$T atoms per square metre with 20% accuracy as discussed in Section 2.3, is therefore an essential part of the diagnostic performance assessment.

The maximum allowed detection limit of the RGA system, defined as three times the standard deviation of the noise, is approximately:

0.96×10^{-7} Pa for Mode 1,
2.53×10^{-7} Pa for Mode 2,
6.46×10^{-7} Pa for Mode 3,
1.66×10^{-6} Pa for Mode 4,
8.29×10^{-6} Pa for Mode 5, and
1.33×10^{-5} Pa for Mode 6.

These estimates assume a tritium inventory of 10 g in the vacuum vessel, uniformly distributed over the vacuum vessel surface, and a total background pressure of 10^{-4} Pa.

4. Optical design and mechanical layout

The T-monitor diagnostic (referred to as the acronym 55.GC in ITER) is planned to be accommodated in Equatorial Port 17. The optical components are distributed across various areas (see Fig. 8a) and consist of both in-vessel and ex-vessel components. The in-vessel components are located within the port, inside the Diagnostic Shielding Module (DSM) [24], specifically in the central DSM#2. Ex-vessel components are located in the Interspace Support Structure (ISS) area, within the bioshield, in the Port Cell Support Structure (PCSS), and in the Tritium building. These groups of optical components do not have a stable common platform, which may result in misalignment between them during operation due to thermal expansion of the optical support structures.

The Fast Scanning Mirror Unit (FSMU) in the ISS, together with the optical dog-leg within the bioshield, plays a key role in aligning the optical system. Alignment checks and corrections will be performed prior to each measurement. Due to space constraints, the size of the optical components is limited. In addition to these size limitations, the long distances also affect optical resolution due to diffraction limits. As the illuminated surface of the divertor must be examined, the same optical system is employed for both launching the high-power laser and collecting the return light for analysis by one of the three integrated instruments. This co-axial configuration accommodates three instruments, each covering different wavelength ranges: a visible (VIS) camera, a near-infrared (NIR) camera, and a 3-pyrometer optical setup, which will be discussed in Section 4.2.4.

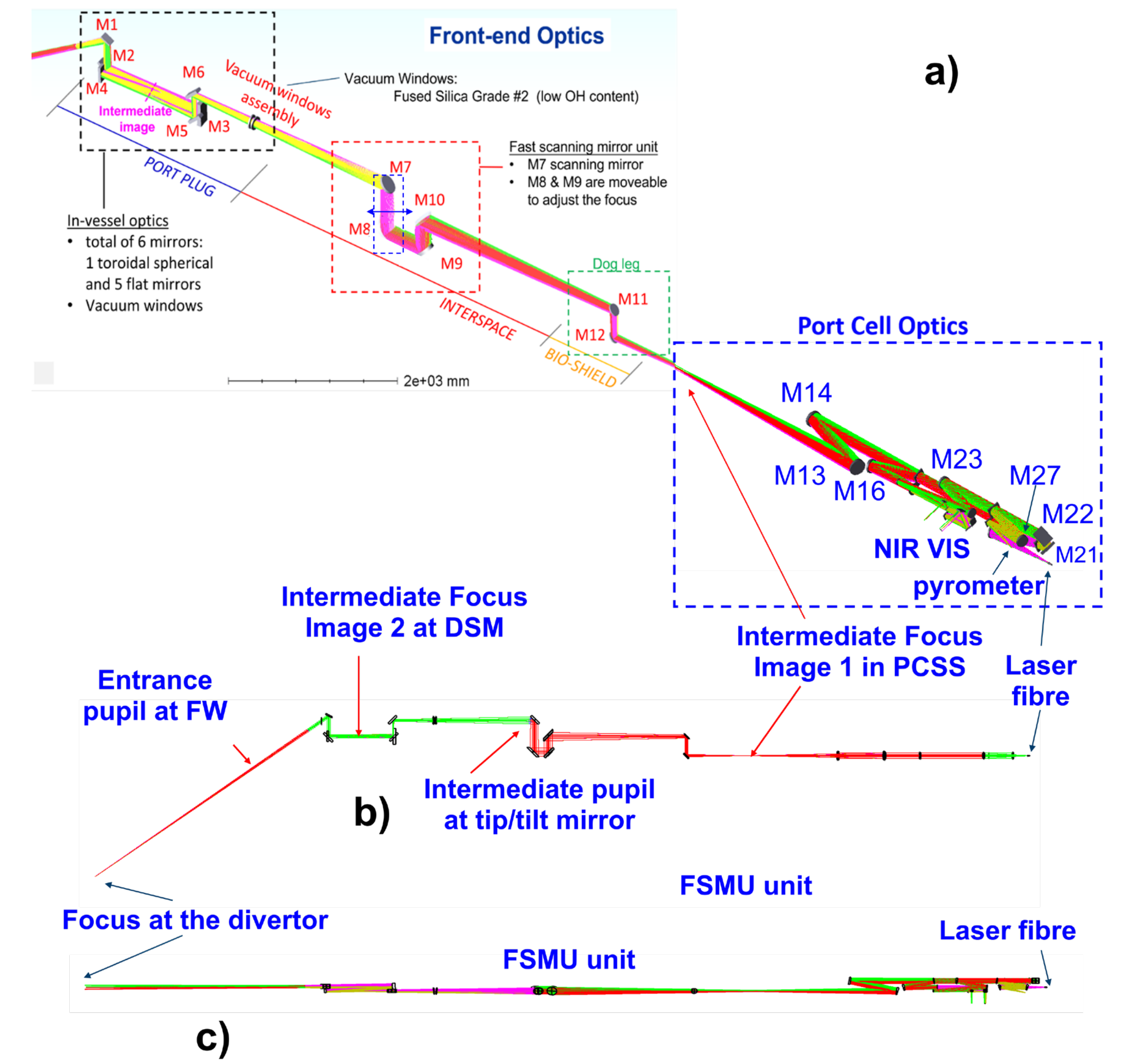

Fig. 8: Overview of the optical layout of the T-Monitor diagnostic system: a) entire optical system; b) Optics for laser beam transport c) Top view of the complete optical system.

Fig. 8a provides an overview of the complete beam path, starting from the laser fiber exit on the bottom right of the picture. The laser fiber diameter is 300 µm, and the required laser spot size at the divertor is 5 mm in diameter. The entrance pupil of approximately 56 mm diameter is located inside the first wall (FW). The size of this pupil is defined by the tip/tilt mirror in the ISS area, as this is where the laser beam positioning at the divertor will be performed. A first intermediate focus plane is placed inside the DSM and positioned between two flat mirrors M4 and M5. The distances between this plane and flat mirrors are defined to maximise the laser beam diameter on these mirrors, thereby reducing the laser power density on their surfaces and minimizing the risk of damage. Due to the tolerances in the DSM, a toroidal mirror will be used, making M3 the imaging mirror. Additionally, the maximum size of the laser beam illumination area of the vacuum window (VW) during full scan of the scanning area must be less than 160 mm, which is the clear aperture of the VW. The DSM intermediate image is reimaged after the

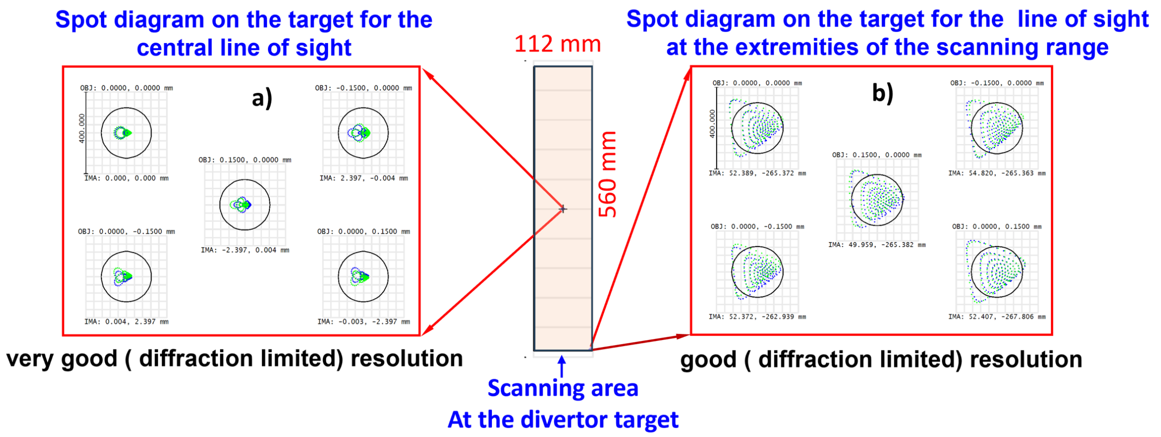

Fig. 9: a) Spot diagram on the target for the central line of sight, with Airy disks shown for comparison b) Spot diagram for the line of sight at the edges of the scanning range.

dog-leg near the bioshield. Reimaging the „Intermediate Focus Image 1“ guides the beams to the focal planes of VIS channel, NIR channel and pyrometer as well as to the laser fibre exit. Fig. 9 shows the spot diagrams for two lines of sight: the central line of sight and the line of sight at the extremities of the scanning area, with Airy disks included for comparison. These diagrams illustrate the distribution of light spots at the divertor baffle (image plane) for given field points at the laser fiber input, highlighting the system's focusing accuracy and the presence of optical aberrations. The Airy disk, representing the smallest achievable spot size due to diffraction, has a radius of approximately 120 µm. The spot diagram sizes for the central line of sight are significantly smaller than the Airy disks, while those for the line of sight at the extremities are comparable in size to the Airy disk. Thus, the optical system is classified as diffraction-limited.

The diffraction-limited resolution of the optical system is determined by the laser wavelength λ and the entrance pupil diameter D, as given by the formula $x = (1.22\lambda/D)\, L$, where L is the distance to the target. In this design D= 56 mm, L= 5.3 m and λ = 1.07 µm therefore the laser spot radius uncertainty is approximately x = 120 µm.

4.1 In-vessel optics

The in-vessel optics comprise six mirrors and a vacuum window, which includes two tilted, uncoated fused-silica discs, each 17 mm thick, as shown in Fig. 10. The system is designed to be ideal in terms of Wavefront Error (WFE) and orientation and it will operate in both forward

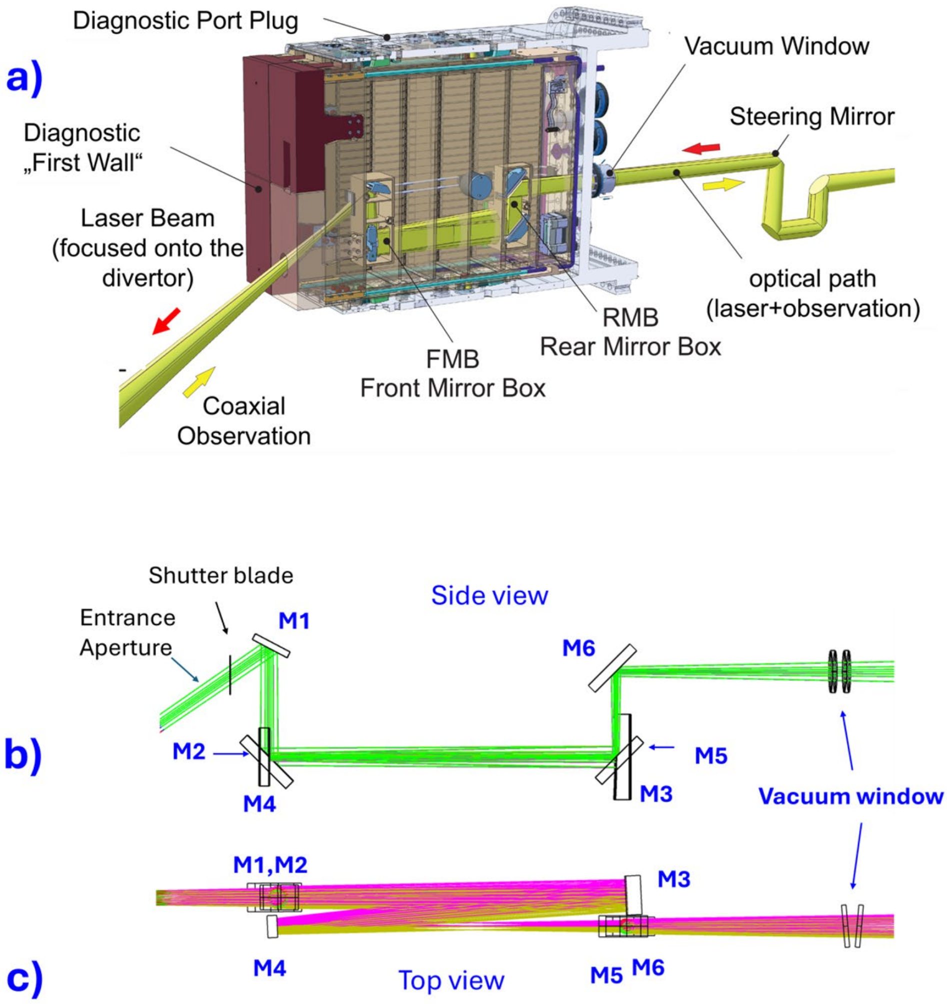

Fig. 10: In vessel optics and shutter a) mechanical layout, b) optical design side view c) optical design top view.

and backward directions. All optical elements are flat, except for mirror M3 which has a toroidal shape. The spacing between the optics is sufficiently large to accommodate thermo-mechanical deformations. Mirrors M1 to M6 are grouped into two separate subassemblies: one containing M1, M2, and M4 (front mirror box (FMB)), and the other containing M3, M5, and M6 (rear mirror box (RMB)), as illustrated in Figures 11 and 12. To ensure neutron shielding, all free spaces in the port plug are filled with B_4C blocks (not shown in the Figures). However, friction between these shielding blocks and stainless steel supports can generate dust inside the port plug. In addition, open shutters from neighboring diagnostics may allow dust from the ITER main chamber to enter, posing a persistent contamination risk. Dust settling on optical components—especially under high-power laser exposure—can cause localized damage, such as pitting or degradation of mirror coatings.

To mitigate these risks, a fully enclosed, dust-tight optical duct is foreseen between the Front Mirror Box (FMB) and Rear Mirror Box (RMB), as shown in Fig. 12. Furthermore, all other critical optical paths within the T-Monitor diagnostic are similarly protected by enclosed housings or ducts to prevent particulate intrusion. Diagnostic shutters are also kept closed during plasma operation to further reduce dust ingress from the main chamber and neighboring systems. Each mirror box in the system is equipped with three thermocouples to monitor temperatures at critical points. One thermocouple is placed in the housing to measure the overall enclosure temperature, and another is located in the mirror holder to monitor the thermal conditions affecting the mirror's structural support. The third thermocouple is embedded in a

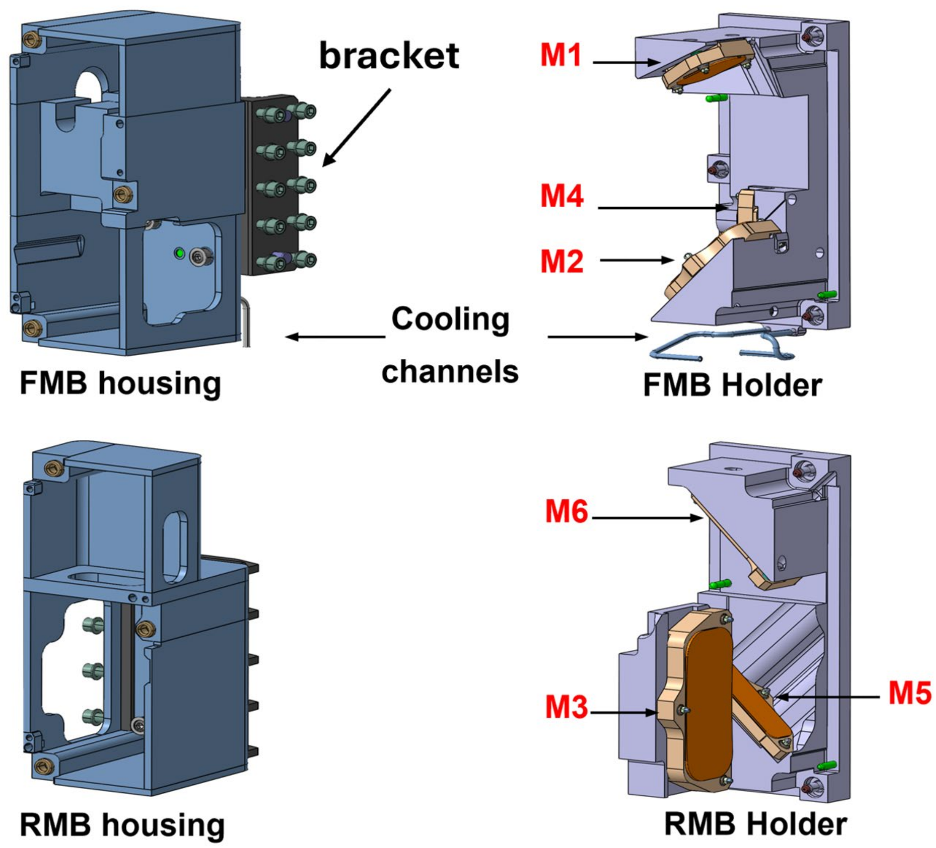

Fig.11: Exploded view of the FMB and RMB components

specific mirror within each box: in the front mirror box (FMB), it is installed into the substrate of the M1 mirror, which faces the plasma environment, while in the rear mirror box (RMB), it is embedded into substrate of M3 mirror, a toroidal-shaped focusing mirror positioned deeper within the optical system. This configuration enables precise temperature monitoring and ensures the protection of these components during laser exposure operation. Type N thermocouples, composed of Nicrosil (Ni-Cr-Si) and Nisil (Ni-Si-Mg) alloys, are favored in high-radiation environments such as ITER [25] due to their robust performance and excellent neutron resistance. They operate in the range of -200°C to 1300°C, with high accuracy at elevated temperatures and minimal drift over time. Their design ensures stability under intense neutron flux, a critical feature for accurate temperature monitoring in nuclear fusion reactors. Unlike some other thermocouples, Type N is less susceptible to degradation or calibration drift under such conditions, making it ideal for long-term use in demanding setups like ITER. Thermocouple extension cables are used to connect thermocouples to their controllers. These cables are made of the same materials as the thermocouple itself: Positive Leg (Nicrosil),

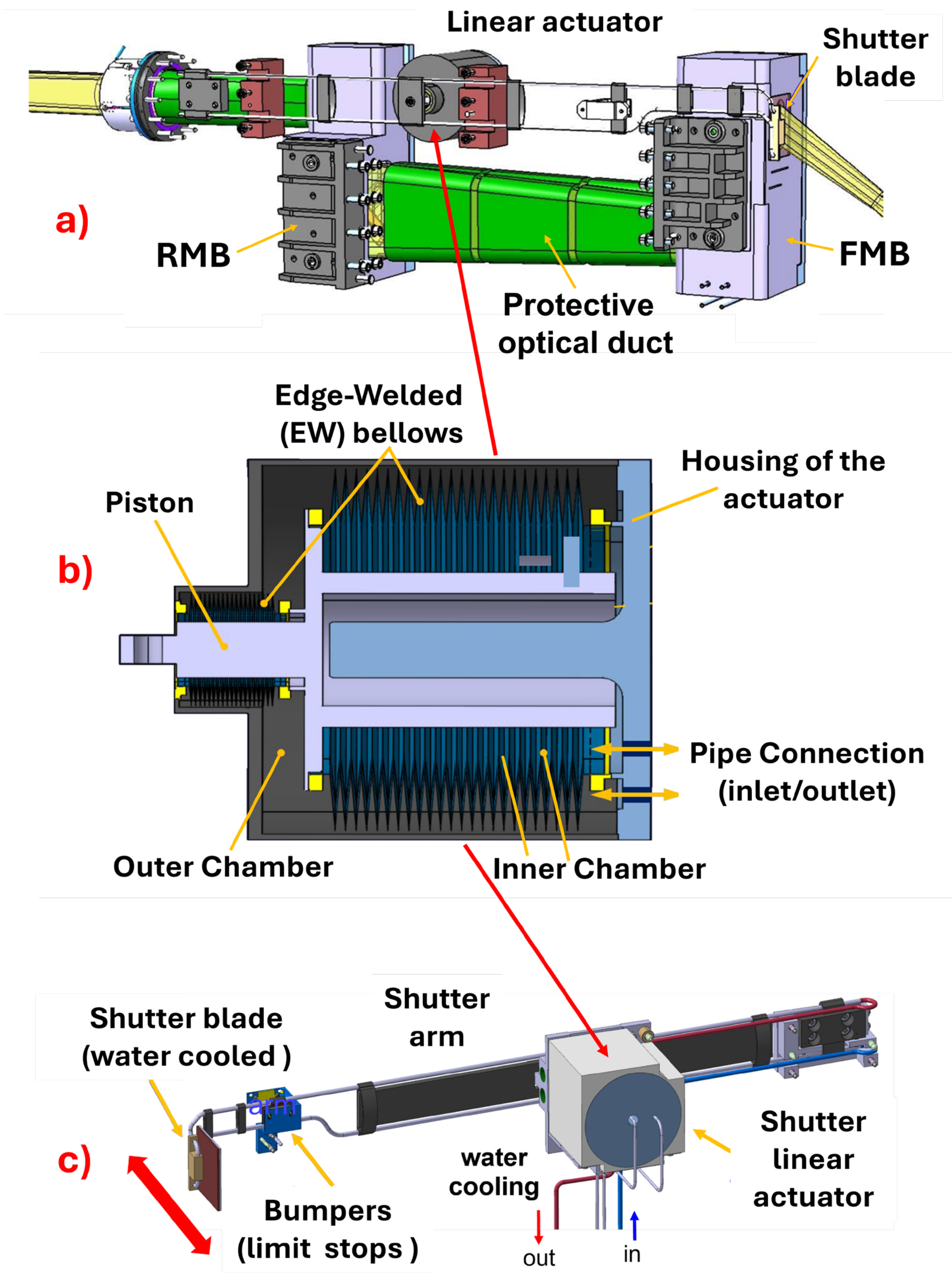

Fig. 12: a) Layout of the boxes with attached mirrors and shutter, b) Actuator cross-section. Inner and outer chamber are separated by a large bellows. The small bellows is the separation of the outer chamber and the port plug environment, c) Shutter assembly

composed of a Nickel-Chromium-Silicon alloy, and Negative Leg (Nisil), composed of a Nickel-Silicon alloy. In demanding environments like ITER, where radiation resistance is critical, these cables are designed with specialized insulation materials. Common options include mineral insulation (used in mineral-insulated or MI cables) and Kapton insulation.

MI cables are widely used in ITER due to their exceptional resistance to high temperatures and radiation. These cables feature metal sheaths (e.g., stainless steel or Inconel) and are filled with magnesium oxide (MgO) insulation, providing outstanding mechanical strength and stability.

In the T-monitor diagnostic system, MI cables were used in the front section of the port plug, where extreme conditions necessitate their durability. Near the feedthrough, cables with Kapton insulation were employed, offering flexibility and reliable performance in moderately demanding conditions.

To verify optical performance, a thermal-mechanical simulation was conducted in ANSYS, considering system assembly, plasma operations, and the Tritium monitor laser scanning. The distorted mirror surfaces from this simulation were analyzed using ray-tracing in Zemax. Reference [26] shows that the system's optical performance criteria meet acceptable limits for spot defocusing and positional shift.

The diagnostic system includes a pneumatic shutter housed within the port plug (Fig. 12) to protect the M1 mirror from deposition and erosion caused by fast neutral particles. The shutter mechanism consists of a linear actuator, a cooled shutter blade, and support arms. Its pneumatic design ensures frictionless operation and high reliability. The shutter and the front mirror box are both equipped with water cooling.

The shutter has a piston stroke of 30 mm, requiring a force of 500 N to open. The support arms have a stiffness of approximately 18 N/mm. The actuator utilizes a two-chamber design, with the chambers separated by edge-welded bellows, forming an inner chamber (IC) and an outer chamber (OC), as illustrated in Fig. 12b. This configuration allows the inner chamber to serve as the primary actuator while the outer chamber partially shields it from environmental effects. Both the inner and outer chambers are maintained at a constant pressure of 0.6 bar during ITER pulses. The actuator is powered by pressurized helium at up to 1.2 bar. To open the shutter, generating an approximate force of 500 N and a piston stroke of about 30 mm, the inner chamber is pressurized from 0.6 bar to 1.0 bar, resulting in a pressure difference of $\Delta p = 0.4$ bar.

Beyond its protective role, the shutter blade is used also to monitor the optical system transmittance at the laser wavelength of 1.07 μm. For this purpose, its rear surface functions as a black body calibration source capable of being heated to 1200°C, with the main laser optionally acting as the heat source. Further details regarding the shutter blade's use as a calibration source can be found in [27]. The shutter blade is equipped with two Type N thermocouples for temperature monitoring during the calibration. Additionally, the shutter arm and shutter actuator are each fitted with thermocouples to ensure precise temperature measurements across the system. The shutter arm is also equipped with a resistive strain gauge element to monitor mechanical strain. Furthermore, the shutter system includes open and closed switches to indicate the operational status of the shutter, ensuring reliable control and feedback for the system.

4.2 Ex-vessel optics

4.2.1 Fast scanning mirror unit in the ISS area

The T-monitor diagnostic is designed to measure the tritium content across the specified spatial range, as shown in Fig. 5 . For precise laser targeting on the divertor baffle, the T-monitor's Fast

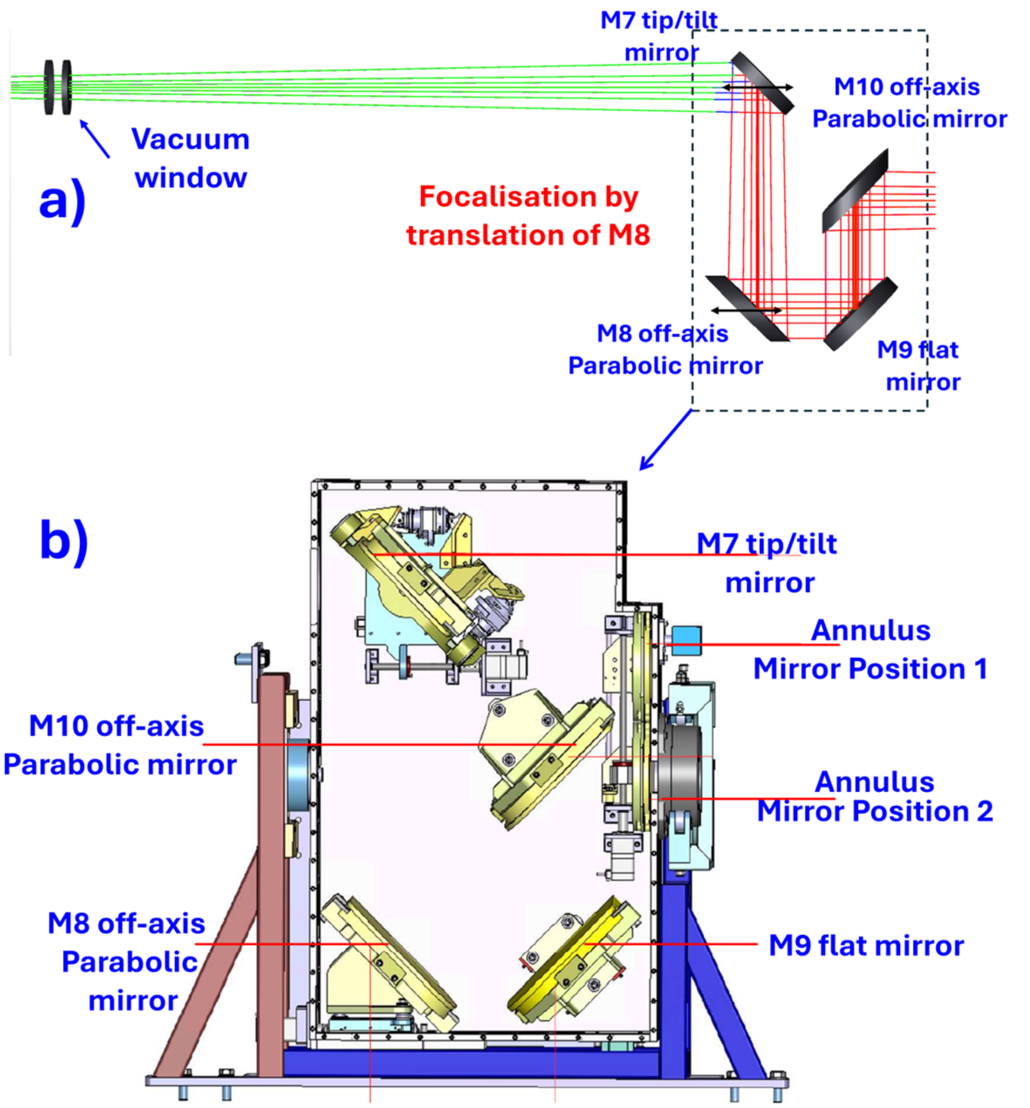

Fig. 13: Fast scanning mirror unit a) optical design and b) the mechanical layout.

Scanning Mirror Unit (FSMU) is an integral component of the diagnostic system, enabling rapid (up to 60 Hz) and precise mirror adjustments. The FSMU, comprising four mirrors, functions as an optical relay between Intermediate Focus Image 1 and Intermediate Focus Image 2.

The M7 beam-pointing mirror offers six degrees of freedom, with vertical tip/tilt angles of ±0.6° and horizontal angles of ±0.16°. To accommodate a 10 mm oversizing of in-vessel mirrors and alignment tolerances, the adjustment range is extended by at least 1° in all directions. This ensures that the operational Line of Sight (LoS) is correctly positioned within the range prior to operation.

Mirror M7 is a flat Zerodur mirror with a gold coating to enhance reflectivity. Focus adjustment at the divertor is achieved by horizontal translation of mirrors M7 and M8, allowing controlled shifts of the line of sight (LoS) and compensation of variations in the focal position of up to 75 mm. Mirrors M8 and M10 are identical 90° off-axis parabolic mirrors with a focal length of 4441 mm whereas M9 is a flat Zerodur mirror.

The use of long–focal-length off-axis parabolic mirrors (M8 and M10) was selected in preference to toroidal mirrors in order to minimize optical aberrations over the full scanning range of the T-monitor system. Toroidal mirrors provide only approximate focusing over a limited field, and optical simulations demonstrated that the associated coma and astigmatism would result in unacceptable spot distortions at the divertor target. In contrast, off-axis parabolic mirrors preserve a high beam quality and an accurate focal spot control, which are essential for reliable laser targeting and precise tritium measurements. The identical focal lengths of M8 and M10 (4441 mm) ensure symmetric imaging conditions and support the use of identical off-axis parabolic elements in the optical layout.

The precision of the scanning mirror system is determined by its tilting step, which adjusts the LoS at the divertor target. This adjustment must be much smaller than the minimum gap between the tungsten (W) blocks (0.5 mm in the poloidal direction). A shift of 0.2 mm corresponds to an M7 mirror tilting angle of approximately 0.0008°. Additionally, the FSMU mirror box can rotate around the optical axis of mirror M10 to compensate for thermal displacements of the port plug in the horizontal direction.

4.2.2 Ex-vessel optics in the bioshield

In the bioshield (Fig. 8a and Fig. 14), a cold dogleg, made up of two flat mirrors (M11 and M12), is positioned to minimize neutron penetration. The alignment of the ex-vessel optics axis with the port plug optics axis is achieved by the combined movement of the FSMU, which involves tilting the FSMU boxes and translating M8, along with the adjustments of the dogleg optics. Each mirror in the dogleg is mounted on a hexapod stage, allowing for remote adjustments with six degrees of freedom.

4.2.3 Ex-vessel optics in the PCSS

Port cells (PCSS) in the ITER fusion device are crucial for housing diagnostic and optical equipment, offering radiation shielding and enabling maintenance access. Within the port cell of the EQ#17, the optical setup of the T-monitor diagnostic combines the laser beam path with the observation path, integrating VIS and NIR cameras, light collection optics for pyrometers, and a laser beam collimator. Fig. 15 shows the coaxial optical system in which the laser path and the observation paths for the VIS and NIR cameras are aligned along a single optical axis. Fig. 15a illustrates the optical design of the system, while Fig. 15b presents the corresponding

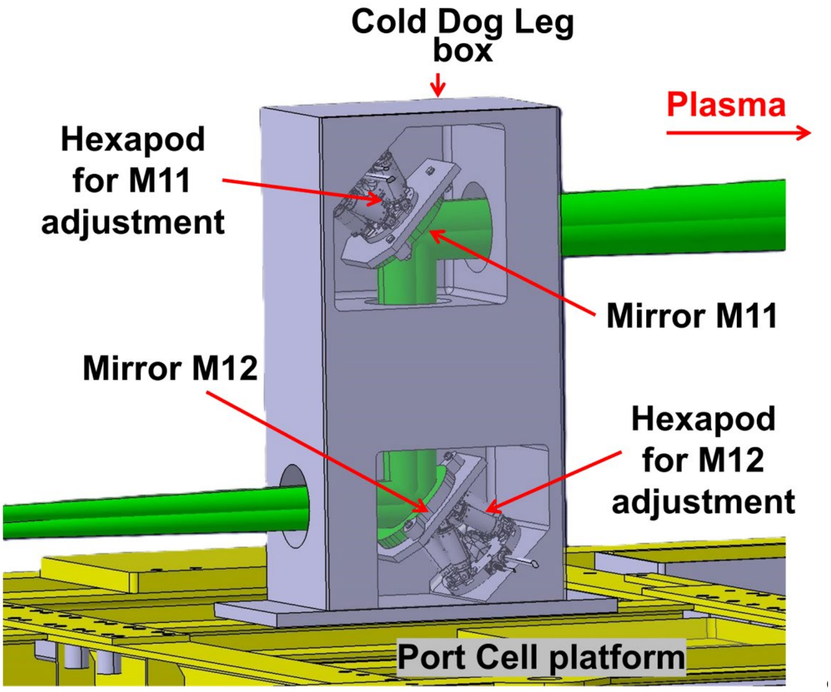

Fig.14 The mechanical layout of the cold leg assembly.

mechanical layout. The system is mounted on a mechanically stable frame with adjustable mounts to enable precise alignment. The laser fibre connector is water-cooled and incorporates an integrated lens for optical aberration correction. The laser beam collimator has a numerical aperture of approximately NA ≈ 0.084.

The VIS camera operates in the wavelength range of 600 nm to 900 nm and provides a maximum field of view of 98 × 98 mm² at the divertor when using a rectangular image sensor with a 1.5-inch diagonal. The camera delivers near-diffraction-limited image quality, achieving an imaging resolution of approximately 0.1 mm at the divertor surface.

The NIR camera covers a wavelength range of 2.1 µm to 2.3 µm, offering a field of view of 12 × 12 mm² at the divertor. Designed for infrared thermal emission detection, this camera supports a frame rate of up to 9.6 kHz with 192 × 192 pixel windowing (FLIR X6980 high-speed MWIR camera, Teledyne FLIR LLC). This capability is essential for monitoring thermal distribution in the target region.

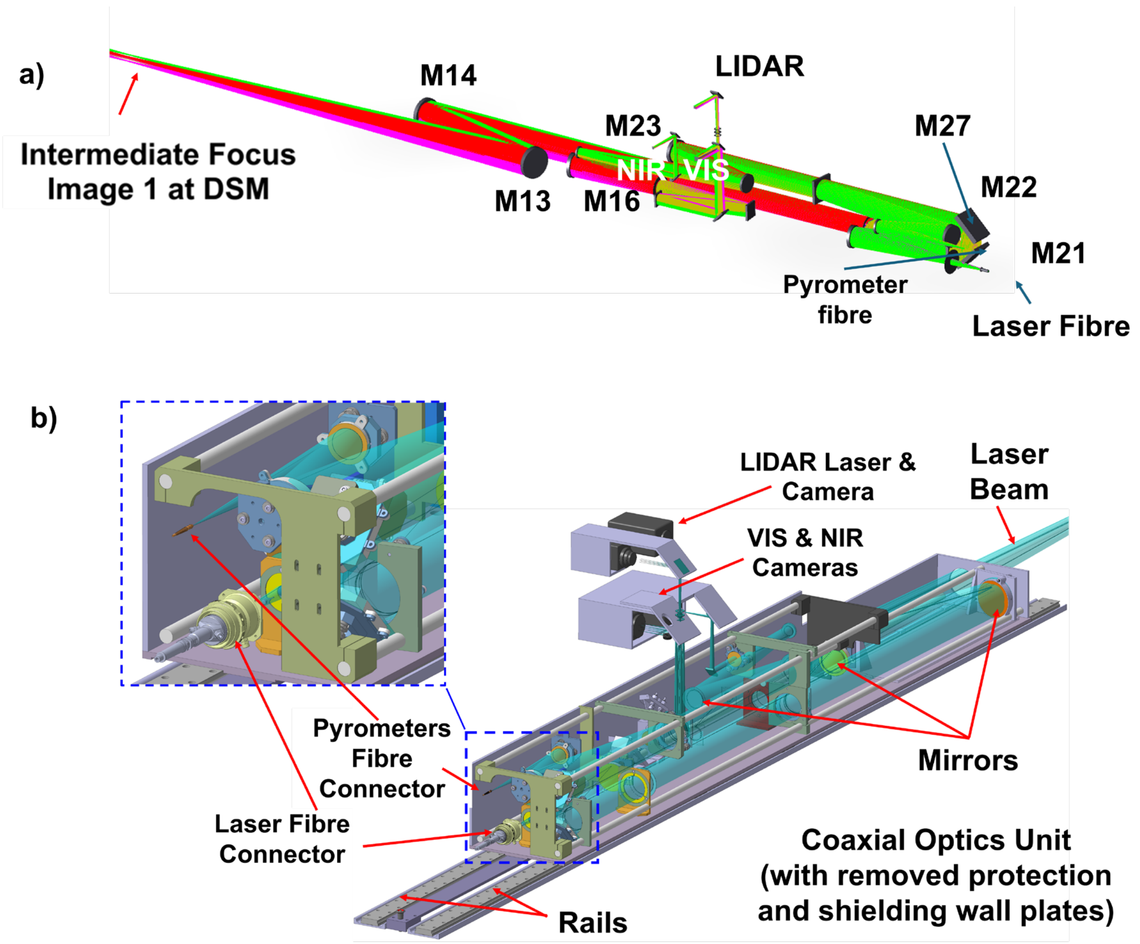

Fig. 15. Coaxial optical system in which the laser path and the observation paths for the VIS and NIR cameras are shown: (a) optical design and (b) mechanical layout.

Radiometric calibration will be performed using a Black Body source positioned at Intermediate Focus Image 2 (refer to Fig. 8b), with temperatures spanning from 400°C to 1000°C. This process, combined with transmittance monitoring of the optical system, will ensure absolute detector calibration and enable assessment of any potential degradation.

4.2.4 Ex-Vessel Components in the T-Building

The Tritium Building houses a high-power laser and an advanced pyrometry system designed to measure temperatures at the laser hotspot on the divertor baffle. The laser transmits light through an optical fibre approximately 30 meters long to the Port Cell Sub-System (PCSS) area, while the pyrometers use separate 30-meter-long fibres to collect IR light accurately from thePort Cell. This separation ensures reliable data collection and minimizes cross-interference.

The pyrometry system consists of three high-speed infrared pyrometers (Pyroskop 840) with a 10 µs time resolution, each tailored for specific subranges of the near-infrared spectrum: 1.4–

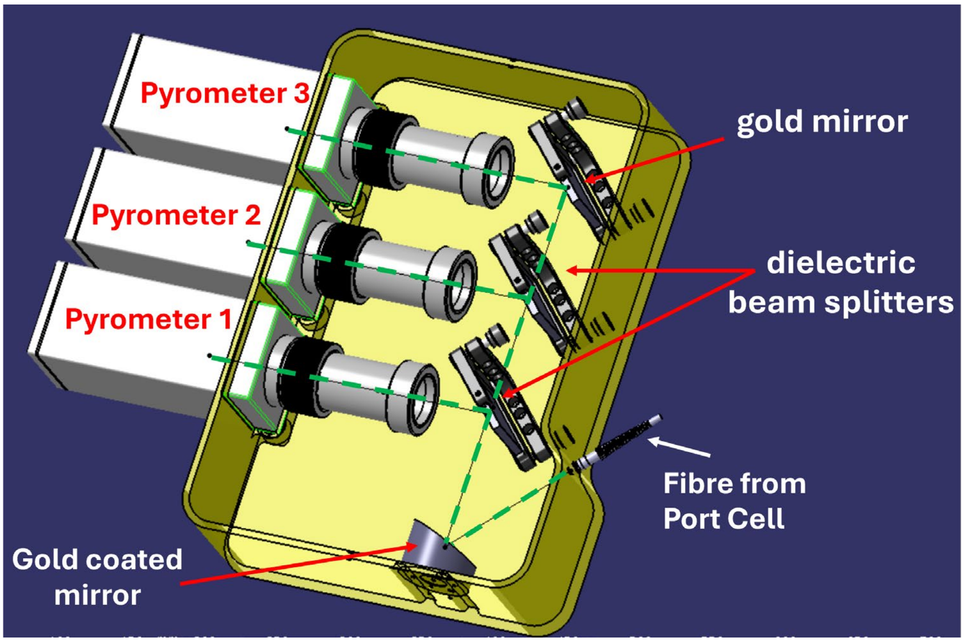

Fig. 16 the pyrometer box with three pyrometers.

1.6 µm, 1.6–1.8 µm, and 1.8–2.0 µm. This setup allows for precise multi-wavelength temperature measurement, crucial for compensating for variations in material emissivity.

IR light from a 4 mm region within the laser hotspot is collected and transmitted via a 400 µm fiber to the optical setup located in the T-Building, as shown in Fig. 16. The fiber channels the light to the pyrometer box, where an intricate arrangement of optical components further processes it. A gold-coated 45° off-axis parabolic mirror with a focal length of 101.6 mm, located inside the pyrometer box, collimates the light into a parallel beam, enabling uniform distribution and efficient splitting.

The beam is then divided into three detection channels by two beamsplitters and plane gold-coated mirror, routing the light to the respective pyrometers (see Fig. 16). Each pyrometer detects its specific spectral range with high accuracy and speed, providing detailed temperature data.

This integrated system delivers precise and reliable temperature measurements, supporting the analysis and monitoring of the laser's impact on the divertor baffle. Its design ensures optimal light collection, processing, and distribution for high spatial and temporal resolution.

A suitable laser for this project is the YLS-Series High Power Ytterbium Fiber Laser from IPG Photonics. It operates at a wavelength of 1070 nm and can deliver up to 60 kW of power in both pulsed and continuous-wave (CW) modes, with pulse durations ranging from 1 to 3 ms. Although the chosen laser is capable of true CW operation, CW is not needed, as the pulsed mode with the selected pulse duration and repetition rate satisfies both the thermal and temporal requirements. The laser requires a high-capacity electrical supply in the T-Building, operating at 400 V, 50 Hz, with a power consumption of 175 kW.

5. Required laser output power and mirror surface materials

As outlined in Section 2, a power density of approximately 665 MW/m² is necessary for a 1 ms laser pulse to fully desorb the hydrogen isotopes from a 100 μm-thick deposited layer. For the chosen laser spot size with a 5 mm diameter, achieving this power density requires a maximum laser power of around 60 kW. This calculation assumes 50% reflectivity of the laser power on the divertor surface and a total optical transmission efficiency of 44%.

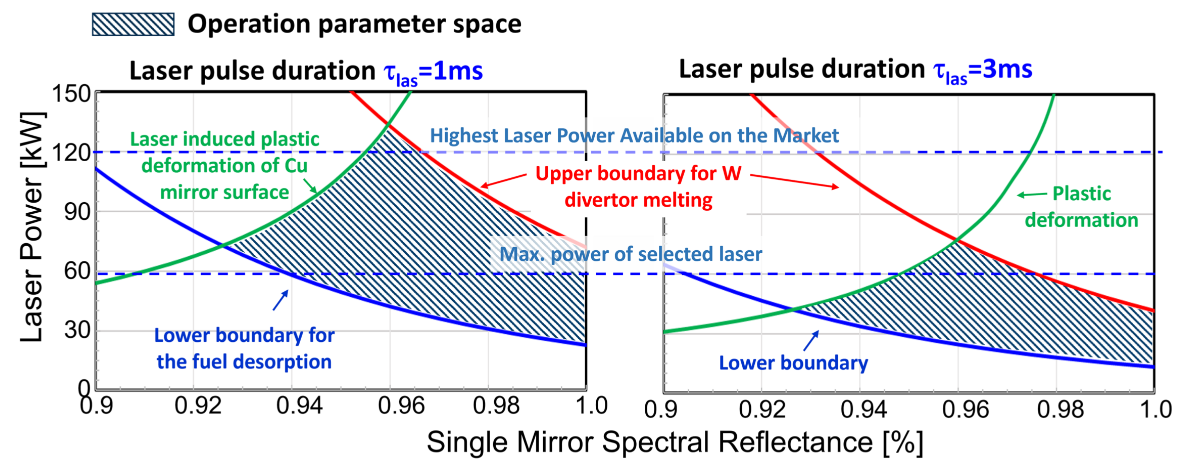

Fig. 17: The operating parameter space in terms of laser power and the reflectivity of a single mirror.

Fig. 17 shows the laser operating parameter space as a function of mirror reflectivity. In this analysis, the laser beam line includes 15 mirrors and one double vacuum window. The mirror surfaces are assumed to be made of annealed copper, representing a conservative case. As discussed in Section 6, annealed copper has a lower heat flux threshold for plastic deformation than pure copper or CuCrZr.

Two operating scenarios are examined, with pulse durations of 1 ms and 3 ms

- The upper boundaries of the operating space (red curves) correspond to the power density at which the divertor material—tungsten in this case—would melt under laser irradiation.

- The lower boundaries (blue curves) indicate the minimum power density required to desorb all hydrogen isotopes in a single laser pulse.
- The left boundary (green curve) represents the maximum allowable power density before the onset of plastic deformation in the mirror substrate. This limit was evaluated using the M4 mirror load case. M4 is one of the mirrors subjected to the highest power density loads in the optical system; it represents, therefore, a critical thermo-mechanical condition. The resulting boundary is conservatively applicable to all CuCrZr mirrors in the in-vessel optical train (M1–M6) as well as to the M11 and M12 mirrors located inside the bioshield.

The threshold for plastic deformation of annealed copper is $\Delta T_{threshold} \approx 11.3°$ C [28, 29].

The selected laser's maximum power of 60 kW fits well within the operating parameter range. However, it is clear that only mirrors with high surface spectral reflectivity (R> 94%) are suitable forour specific application.

Figure 18 presents the spectral reflectivity of various materials commonly used in fusion devices. The data used for the evaluation of the spectral reflectivity are taken from [30]. The materials selected for comparison include metals with diverse optical properties, such as gold (Au), silver (Ag), aluminum (Al), copper (Cu), rhodium (Rh), molybdenum (Mo), nickel (Ni),

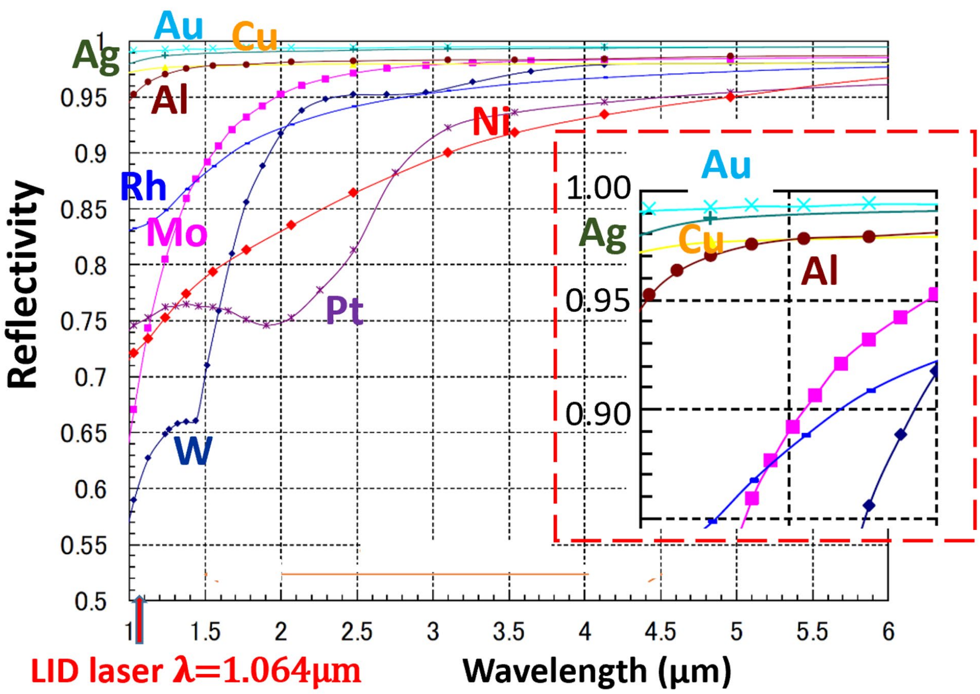

Fig. 18 Spectral reflectivity of the following materials: gold (Au), silver (Ag), aluminum (Al), copper (Cu), rhodium (Rh), molybdenum (Mo), nickel (Ni), platinum (Pt), and tungsten (W).

platinum (Pt), and tungsten (W). As shown in Figure 18, for the LID laser operating at a wavelength of λ = 1.064 µm, the most suitable materials are Au (R ≈ 99%), Ag (R ≈ 98.5%), Cu (R ≈ 97%), and Al (R ≈ 96.5%). Despite their high reflectivity, Ag and Al can activate into very long-lived isotopes, which makes them less practical for this application. As a result, Au and Cu emerge as the most viable options.

In our project, gold and copper were chosen as coatings for all metallic mirrors in the beam path due to their excellent and consistent reflectivity in the infrared wavelength range. These coatings also provide high reflectivity in the visible spectrum down to approximately 550 nm. This ensures optimized reflection of the high-power laser (97–99%) while maintaining sufficient reflectivity for the pilot laser and the visible feedback image. The pilot laser, used to visualize the main laser's spot location on the divertor tiles, will operate at a wavelength of approximately 660 nm.

6. Required Mirror Substrate Material

High-power laser illumination can cause transient surface heating, inducing significant stresses inside the mirrors. These stresses may lead to surface roughening, yielding (plastic deformation when the stress exceeds the yield strength), or fracture.

Key criteria for material selection are:

Stress Resistance and Yield Strength: Materials should possess sufficient yield strength to withstand the transient stresses induced by high-power laser heating. If the stress exceeds the yield strength, plastic deformation or fracture may occur. The material's ability to resist these stresses is critical in preventing damage during laser exposure. The critical heat flux factor, $Q_{f,crit}$, is defined as the threshold at which the stress equals the yield strength and plastic deformation occurs. The heat flux factor is defined as $Q_f = q\sqrt{t}$, where q is the surface heat flux and t is the laser pulse duration.

Thermal Conductivity and Heat Penetration: Materials should have appropriate thermal properties, such as high thermal conductivity and suitable thermal diffusivity, to ensure efficient heat dissipation. This helps prevent excessive heating that could cause surface deformation or failure. The heat penetration depth needs to be sufficient to manage the laser-induced temperature rise without leading to detrimental effects like surface roughening.

Surface Deformation and Damage Resistance: Materials must maintain structural integrity under thermal expansion induced by laser irradiation. Deformation factors should remain within acceptable limits (e.g. not exceeding a $\lambda/8$ wavefront error) to prevent optical performance degradation. The heat flux threshold at which the λ/8 wavefront error occurs is defined in this paper as $Q_{f,\lambda/8}$. Materials should also resist failure modes such as coating delamination (e.g., for gold coatings at 500°C) and prevent plastic deformation or surface roughening due to thermal expansion.

Accurate stress determination for specific materials and loads often requires time-dependent, 3D analysis. However, in many cases, a simplified model assuming two-dimensional constraints and no constraints in the third dimension provides a good estimate of peak stress [28]. For most materials, the value of $Q_{f,\lambda/8}$ is lower than the plastic deformation threshold ($Q_{f,\lambda/8} < Q_{f,crit}$) . However, materials like annealed copper experience plastic deformation before reaching λ/8.

In this project, the following materials have been selected as mirror substrates:

- For the in-vessel mirror and optical components inside the biological shield, CuCrZr coated with gold is used. The maximum heat flux factor on the in-vessel mirror is experienced by the M5 mirror, with a heat flux factor of about 0.26 $MW/m^2 \cdot s^{1/2}$. The critical heat flux factor, $Q_{f,crit}$, for CuCrZr alloys allowed at ITER [31] varies between 1.6 and 3.8 $MW/m^2 \cdot s^{1/2}$: 1.6 $MW/m^2 \cdot s^{1/2}$ for grade C, 2.7 $MW/m^2 \cdot s^{1/2}$ for grade B, and 3.8 $MW/m^2 \cdot s^{1/2}$ for grade A. Therefore, the $Q_{f,crit}$ for the potential damage to the mirror is larger than the experienced heat flux factor. On the other hand, the critical heat flux factor for achieving λ/8 deformation in CuCrZr is lower than that for plastic deformation: $Q_{f,\lambda/8}$=0.44 $MW/m^2 \cdot s^{1/2}$. Thus, we will operate at a heat flux factor approximately half the value of $Q_{f,\lambda/8}$.

- For ex-vessel optical components, we will use Zerodur as the substrate material, coated with gold. The critical heat flux factors $Q_{f,crit}$ and $Q_{f,\lambda/8}$ are very high, 12.3 $MW/m^2 \cdot s^{1/2}$ and 100 $MW/m^2 \cdot s^{1/2}$, respectively. In these cases, coating delamination will occur before reaching these critical heat flux factors. When the gold (Au) coating reaches 550°C, delamination of the Au layers from the substrate is expected, leading to coating failure. Substrates made of Zerodur will reach 550°C before hitting the critical heat flux factors for λ/8 or plastic deformation. The heat flux factor at which the gold coating reaches T = 550°C is $Q_{f,\Delta T=500°C}$ = 0.8 $MW/m^2 \cdot s^{1/2}$, which is much lower than $Q_{f,crit}$ and $Q_{f,\lambda/8}$.

8. Operating Modes for T-Retention Measurements

Tritium monitoring operations commence 6 hours after a series of ITER plasma pulses. By this time, the temperature distribution in the Diagnostic Shield Module (DSM) has nearly reached equilibrium. The tritium monitoring process involves high-power laser irradiation of the divertor tiles, inducing desorption of tritium, which is then analyzed using Residual Gas Analysis (RGA) to monitor the partial pressures of hydrogen isotopomers. During laser irradiation of a single monoblock or a set of monoblocks, the number of laser pulses per measurement is determined by the selected operating mode, as outlined in Table 1.

The values in the table represent the incident power (energy) delivered to the target. A portion of this power is reflected from the target surface, while the remainder is absorbed. For example, the incident power required to melt a beryllium deposit layer is approximately 26 kW for a laser spot with a 5 mm diameter and a 1 ms pulse duration. This results in a temperature increase of about $\Delta T = 1200$ K, assuming an absorption coefficient of tungsten of 0.5. Under these conditions, the absorbed power density is around 665 MW/m², which represents the most critical case requiring the maximum incident power.

Mode	Number of laser pulses	Laser pulse frequency [Hz]	Total energy on tile 1ms (3ms) [J]	Average power on tile 1ms (3ms) [kW]
1	1	-	25.8 (44.7)	25.8 (14.9)
2	3	0.67	77.5 (134)	0.0258 (0.0447)
3	8	2.3	207 (358)	0.0689 (0.119)
4	24	7.7	620 (1074)	0.207 (0.358)
5	120	40	620 (1074)	1.03 (1.79)
6	192	64	620 (1074)	1.65 (2.86)

Table 1: Parameters of the laser system and the power loads applied to the divertor tile for all planned laser operation modes. The table includes two possible pulse durations: 1 ms and 3 ms.

Deposits on the tungsten surface reduce laser beam reflection, thus increasing absorption. Additionally, the effect of inclined laser incidence on reflection can be neglected within the intended angular scanning range of ±40° [32]. Consequently, the reduced reflection and increased absorption coefficient allow for lower required incident laser power, which can be adjusted during measurements.

The operating mode depends on the tritium content retained in the wall. If the tritium content is high, Mode 1 is used, which involves a single laser pulse. If the content is insufficient, additional laser pulses are applied at different tile locations. This ensures that the amount of tritium released exceeds the sensitivity threshold of the measurement sensors, ensuring accurate measurements. Notably, in Mode 4, the sensitivity increases by a factor of 17.6 compared to Mode 1.

Figure 19 illustrates the laser spot sizes for scanning modes up to Mode 4. Mode 4 represents a full scan of a single monoblock with 24 laser spots. Additional modes—Mode 5 (120 laser pulses) and Mode 6 (192 laser pulses)—represent the same scanning procedure for 5 and 8 monoblocks, respectively.

In modes higher than mode 1, the scanned area is significantly larger than the individual laser spot, ensuring that outgassing originates from the entire region covered by the scan. In these modes, the objective is to quantify the total deuterium released from the deposit during the complete sequence of pulses defined for that mode rather than resolving the desorption associated with individual pulses. To maintain an RGA measurement accuracy better than 10%, the total duration of the pulse sequence for each mode is limited to approximately 3s, which is substantially shorter than the vacuum vessel pumping time of 20 s. This requirement determines the specific laser repetition rate frequency applied in each mode so that the full pulse sequence fits within this 3 s window, ensuring that the integrated outgassing signal is measured reliably without significant influence of the pumping dynamics.
To achieve this, the exposure points need to overlap. A step size equal to the laser spot diameter divided by √2 is used to ensure optimal coverage of the exposed monoblock surfaces.
Please note that the total measurement time for each mode should remain under 3 seconds. This requires an increasing laser pulse frequency as the modes progress. In Mode 6, the highest required frequency is 64 Hz.
The total absorbed power per 3 ms laser pulse ranges from 570 W for the M1 mirror to 703 W for the M6 mirror, accounting for a surface reflectivity of 96%. However, the most critical

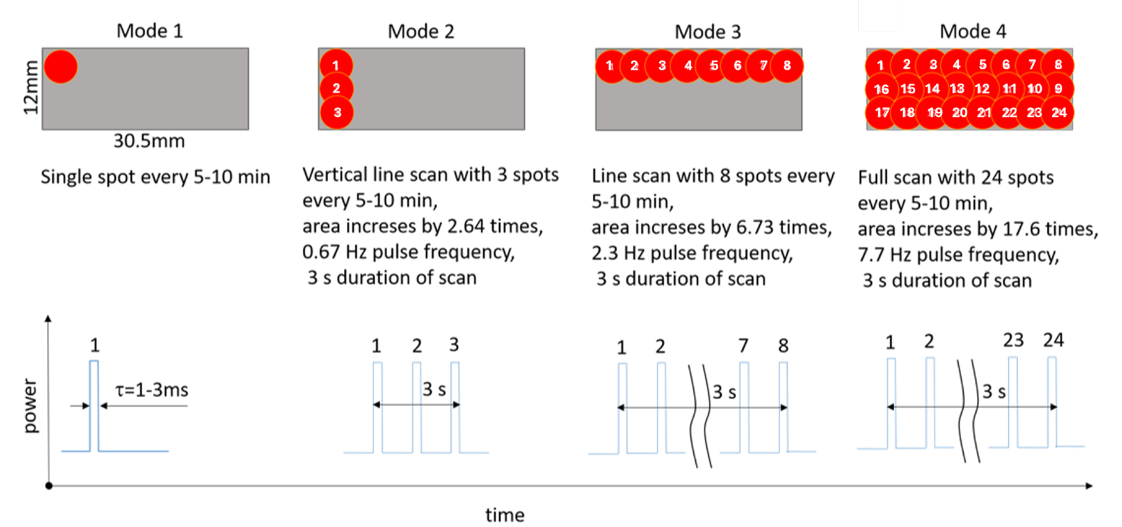

Fig.19: Several modes for the laser scan of monoblocks' top area.

parameter is the power density. Since the M4 mirror has the smallest laser spot footprint, it experiences the highest incident power density, approximately 14 kW/cm². The absorbed power for M4 per 3 ms laser pulse is 650 W, leading to a cumulative absorption of 9.4 kJ over 192 pulses.

Figure 20a illustrates the temperature distribution after a 6-hour cooldown following plasma operation, while Figure 20b presents the resulting temperature distribution for M4 at the end of the 192nd pulse. Before the T-monitor measurements, the temperature of the M4 mirror is nearly uniformly distributed, with a temperature deviation of less than 0.1°C. After the 192nd laser pulse, the maximum temperature increase is less than 8°C, remaining below the threshold for plastic deformation of annealed copper ($\Delta T_{threshold} \approx 11.3$°C).

Additionally, Figure 20c depicts the total deformation after the 192nd pulse (in micrometers, considering only the laser load). Ray-tracing analysis conducted in Zemax, using the distorted mirror surface of M4, indicates that the deformation does not significantly affect image quality compared to the nominal case [26]. Minor spot position shifts caused by surface deformation can be corrected through readjustment (corrected focusing with help of FSMU) before the next laser pulse is issued.

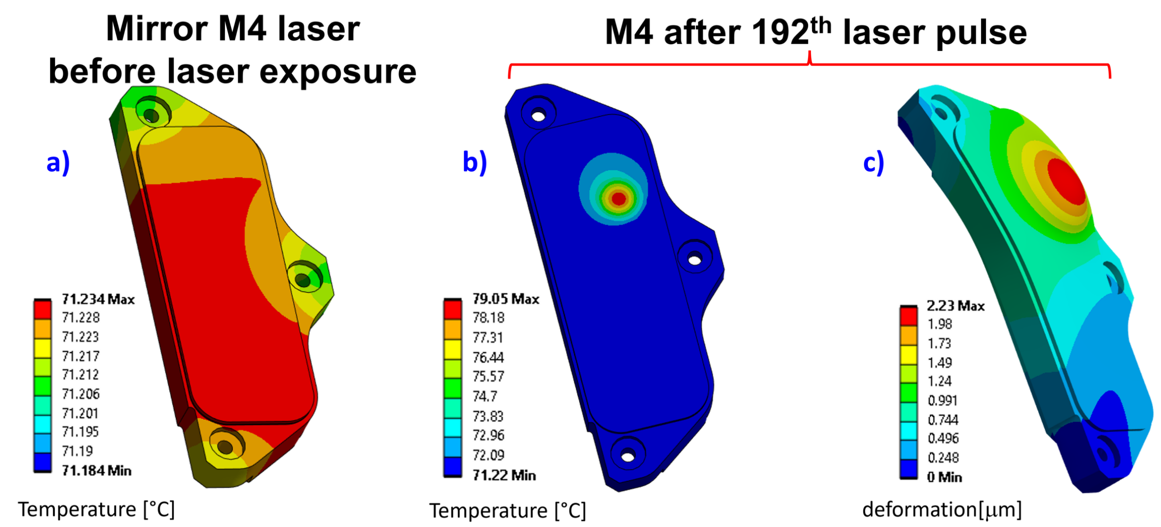

Figure 20: (a) Temperature distribution after a 6-hour cooldown following plasma operation; (b) Temperature distribution after the 192nd pulse for M4; (c) Total deformation after the 192nd pulse (in micrometers, considering only laser load).

8. Monitoring Transmittance of Optical Beam Path Using Black Body Calibration

The transmittance of the entire optical beam path is monitored using a black body plate mounted on the backside of a shutter blade. This plate, coated with a high-emissivity material, is heated by a 1.0 kW continuous-wave (CW) laser beam, which raises its temperature up to 1000°C. The elliptical plate measures 81 mm by 94 mm in size. The plate's temperature is accurately monitored by a thermocouple integrated into the black body plate. Emission from the black body plate, at several fixed temperatures, is detected by all optical sensors in the T-monitor system. For system calibration, the black body calibration plate is used to measure the transmittance of the T-monitor optics in the Port Plug across the entire wavelength range, including the 1.07 μm wavelength of the heating laser. Additionally, a second black body calibration source is placed at the first intermediate image of the laser fiber end. By comparing the calibration of the black body shutter plate with the calibration source at the intermediate image, the system can assess the degradation of optics in the Port Plug and ISS areas.

The T-monitor diagnostic is designed to monitor the laser power exiting the laser fiber connector. This monitoring will be performed using a calorimeter (Compact Power Monitor CPM F-30 from PRIMES company [33]) capable of measuring a maximum power of up to 30kW. To measure the laser power, an additional mirror will be temporarily moved into the laser beam path, redirecting the beam into the calorimeter.

When no measurements are being conducted, the calorimeter will function as a laser beam dump, safely absorbing any laser energy in the event the laser beam is accidentally activated. For safety reasons, the mirror will remain positioned in the beam path by default unless measurements are underway. The F-30 must be cooled with a water flow rate of 25 to 30 liters per minute, with a water pressure of 3 bar in the cooling circuit.

9. Summary

Tritium inventory control is a critical safety and licensing requirement for ITER, which must limit the on-site tritium retention to 1 kg. One of the most uncertain and challenging contributors to this inventory is co-deposited tritium on divertor surfaces. Accurate, spatially resolved diagnostics are essential to quantify this retention and support detritiation strategies, ensuring both operational safety and regulatory compliance.

This paper presents the development of a novel in-situ diagnostic system—the T-monitor—designed by Forschungszentrum Jülich to measure tritium retention on divertor tiles under ITER-relevant conditions. The system combines Laser-Induced Desorption (LID) with Quadrupole Mass Spectrometry (QMS) to quantify the hydrogen isotope content with high spatial resolution, without requiring component dismantling.

For ITER, the T-monitor enables measurements of hydrogen isotopes (H, D, T) on the divertor inner baffle, covering a concentration range of 1.0×10^{21} to 2×10^{24} with 20% accuracy. Tritium retention arises mainly from co-deposition with boron/tungsten and implantation into tungsten, with projected retention reaching up to 380 g by the end of the DT-1 phase. Accurate quantification requires detection of multiple tritium-containing species (e.g., T_2, DT, HT, HTO), necessitating a Residual Gas Analyzer (RGA) with fast response (<2 s) and high mass resolution.

The T-monitor optical system employs a coaxial design to deliver the high-power laser and collect diagnostic signals through shared optics. The returning light is routed to a visible camera, a NIR camera, and pyrometers, enabling thermal imaging and precise temperature monitoring during desorption. These cameras deliver near-diffraction-limited imaging, achieving ~0.1 mm resolution at the divertor surface.

The optical path includes six in-vessel mirrors (one toroidal), a vacuum window, and ex-vessel relay optics (21mirors in total) with a fast scanning mirror unit, the FSMU (§4.2.1). It achieves diffraction-limited performance, with a ~120 μm spot radius uncertainty over the 5.3 m beam path, ensuring high spatial resolution.

The front-end optics include six high-reflectivity mirrors (>96%) with stress-tolerant gold and copper coatings. In-vessel and dog-leg mirrors use CuCrZr substrates for thermal and mechanical resilience, while Zerodur is used ex-vessel for thermal stability and optical precision. The Fast Scanning Mirror Unit (FSMU) enables scanning of the inner baffle area (±0.27 m poloidally, ±0.055 m toroidally), using gold-coated Zerodur mirrors with fine tip/tilt control and focus adjustment. The FSMU provides fast (up to 60 Hz), sub-millimeter beam steering.

Key technical features include a 60 kW near-infrared laser, optimized for desorption with a pulse duration of 1–3 ms and a 5 mm spot size on target (the divertor inner baffle). The laser heats the targeted areas to ~1600 K, desorbing hydrogen isotopes that are analyzed by the QMS.

The system includes a frictionless pneumatic shutter and is engineered for remote handling, high magnetic fields, and the thermal loads expected in ITER. In-situ calibration using a heated blackbody plate allows monitoring of the degradation of the optical path components and of the detector sensitivity over time.

Multiple operational modes ensure robust, localized diagnostics during diagnostic operation across a wide range of tritium concentrations, maintaining 20% accuracy and fine spatial resolution.

In summary, the T-monitor is a robust, ITER-compatible system for localized in-situ tritium inventory diagnostics during operation. Its deployment represents a key advancement in supporting safe, sustained fusion operations and meeting regulatory requirements by reducing the uncertainty in fuel retention.

Acknowledgments

This work is supported by the ITER Organization under the Cooperation Agreement between Forschungszentrum Jülich GmbH and ITER (ref. IO/21/CT/4300002506). The views expressed do not necessarily reflect those of the ITER Organization.

References

[1] De Temmerman G. *et al* 2017 *Nucl. Mater. Energy* **12** 267-272
[2] Pitts R. A. *et al* 2025 Nucl. Mater. Energy **42** 101854
[3] Carpentier S. *et al* 2011 *J. Nucl. Mater.* **415** S165
[4] Schmid K. *et al* 2015 *Nucl. Fusion* **55** 053015
[5] Schmid K. *et al* 2024 Nucl. Mater. Energy **41** 101789
[6] Loarte A. *et al* The new ITER Baseline, Research Plan and open R&D issues, submitted to Plasma Phys. Control. Fusion.
[7] Zlobinski M. *et al* 2019 *Nucl. Mater. Energy* **19** 503–509
[8] Huber A. *et al* 2001 *Phys. Scr.* **T94** 102-105 doi :10.1238/Physica.Topical.094a00102
[9] Schweer B. *et al* 2009 *J. Nucl. Mater* **390–391** 576-580
[10] Zlobinski M. *et al* 2024 *Nucl. Fusion* **64** 086031
[11] Klepper C. C. *et al* 2022 *IEEE Trans. Plasma Sci.* **50** /12 4970-4979.
[12] Zlobinski M. *et al* J. Nucl. Mater **438** S1155-S1159
[13] Carslaw H. S., Jaeger J. C. , Conduction of heat in solids (2nd edition), Clarendon Press, 1959
[14] Villari R. *et al* 2013 Fusion Eng. Des.88 2006– 2010
[15] Schwarz-Selinger T. *et al* 2023 Mater. Res. Express **10** 102002
[16] Ogorodnikova O.V. and V.Gann 2015 J. Nucl. Mater. **460** 60–71
[17] Yu J. H. *et al* 2017 Nucl. Mater. Energy **12** 749-754
[18] Huber A. *et al* 2017 Phys. Scr. **T170** 014027 (7pp)
[19] Thomas L. K. J. Appl. Phys., 1968, **39**, 4681–4686
[20] Sub-System Requirement Document sSRD-55.GC: Tritium Monitor https://user.iter.org/?uid=WYWX2X
[21] Romazanov J. et al. 2024 Nucl. Fusion 64 086016 https://doi.org/10.1088/1741-4326/ad5368
[22] Hirai T. *et al* 2016 *Nucl. Mater. Energy* **9** 616-622 doi:10.1016/j.nme.2016.07.003
[23] B. Quinlan *et al*, submitted to Nuclear Fusion and under review
[24] Burdakov A. *et al* 2022 *Fusion Eng. Des.* **178** 113114
[25] Nieuwenhove Van R. and Vermeeren L. Rev. Sci. Instrum. 75, 75–83 (2004)
[26] Ivashov I. *et al* 2025 *Fusion Eng. Des.* **220** 115295
[27] Friese F. *et al* submitted to Fusion Eng. Des. 2024
[28] Blanchard J.P. 2003 *Fusion Science and Technology* **44** (1) 101-105. https://doi.org/10.13182/FST03-A317
[29] Arakcheev A. S. *et al* 2015 *J. Nucl. Mater* **463** 246-249.
[30] https://refractiveindex.info/?shelf=main&book=Au&page=Magnozzi-25C

[31] Appendix A, Materials Design Limit Data, https://user.iter.org/?uid=222RLN

[32] L. K. Thomas, Journal of Applied Physics (1968) **39,** 4681-4686.

[33] https://www.primes.de/en/products/laser-power/continuous-radiation/compactpowermonitor-cpm.html